

An Analysis of the Affinity and Stability of Base Pair Changes of the  
Glucose-Binding and Cocaine-Binding Aptamers

Meghan T. Osborne

A DISSERTATION SUBMITTED TO THE FACULTY OF GRADUATE  
STUDIES IN FULFILLMENT OF THE REQUIREMENTS FOR THE DEGREE  
OF MASTERS OF BIOLOGY

GRADUATE PROGRAM IN BIOLOGY  
YORK UNIVERSITY  
TORONTO, ONTARIO

August 2023  
©Meghan T. Osborne 2023

## Abstract

Aptamers are selected to bind to their ligands, usually with high affinity and selectivity for targets. An aptamer was previously selected to bind glucose with a  $K_d$  of 10mM which is physiologically relevant as the blood glucose concentration typically falls between 4-11 mM. NMR spectroscopy is suited to study weak aptamer-ligand interactions and was used to investigate the affinity of sequence modified glucose-binding aptamers to try and determine a sequence with a greater binding affinity. Three of thirteen modifications bound to glucose, the change of a G-T base pair to a G-C base pair (Glumod-7) with a  $K_d$  of  $2.9\text{mM} \pm 0.3\text{mM}$ , the alteration of the terminal triloop from a C-T-C to a G-A-A (Gumod-8) with a  $K_d$  of  $12\text{mM} \pm 3\text{mM}$ , and the truncation by 3 base pairs (Glumod-12) which was too weak to determine a  $K_d$ . Glumod-7 was the only sequence which had a comparable  $K_d$  and would require further investigation in terms of stability using NMR thermomelts. Cocaine-binding aptamers are intriguing as they are composed of three stems centered around two mismatch A-G base pairs and are very well studied in terms of secondary structure and affinity. The thermostability of cocaine-binding aptamers as a function of number of base pairs in stem one was investigated by DSC. There was a trend observed of increasing in stability from 1 base pair to 6 base pairs with a decrease seen at 7 base pairs. The most thermodynamically stable aptamer was determined to be MN4, a preformed structure.

## **Acknowledgements**

I would like to thank my family and friends for being constant pillars of support through the years. A special thanks to my mother who without her love and advice none of this could've been possible. A thank you to her for spending countless hours with me on the phone with nothing but words of encouragement throughout the years. Without her none of this could've happened. A notable thank you to Tyra Bain who I would not have survived these years without her friendship.

A heartfelt thank you to my supervisor Philip Johnson for granting me access to the knowledge of his lab. Thank you for allowing me the space and freedom to grow as a scientist while also supporting my critical thinking journey. Thank you for the kind lab environment which you have cultivated. Thank you for allowing me to be a part of your lab for the last 2 years. I want to thank my committee member Andy White for his advice and feedback on my work.

Thank you, Yunus Kaiyum, for being a supportive mentor and being my constant source of support, advice, and knowledge. I also want to thank Zach Churcher for expanding my knowledge and being a support in my education. Furthermore, Emily Chao I appreciate your support and endless hours of laughs throughout our masters. Thank you, all Johnson Lab members, past and present for their help and company.

## Table of Contents

Abstract	II
Acknowledgements	III
Table of Contents	IV
List of Tables	VI
List of Figures	VII
List of Abbreviations	IX
Chapter One: Background and Introduction	
1.1 Introduction to Aptamers	11
1.2 SELEX	12
1.3 Aptamer Structure	13
1.4 Aptamer Applications	15
1.5 The Cocaine-Binding Aptamer	17
1.6 The Glucose-Binding Aptamer	24
1.7 Differential Scanning Calorimetry	28
1.8 NMR Spectrometry	30
1.9 Thesis Project	32
Chapter Two: Methods and Materials	
2.1 Preface	33
2.2 Aptamer Preparation	33
2.3 Ligand Preparation	33
2.4 DSC Equipment Setup	33
2.4.1 General	33
2.4.2 Data Analysis	34
2.5 NMR Equipment Setup	35
Chapter Three: Affinity Analysis of Modified Glucose-Binding Aptamers	
3.1 Preface	37
3.2 Introduction	37
3.3 Results and Discussion	40
3.4 Concluding Remarks	60
Chapter Four: Thermodynamic Properties of Cocaine-Binding Aptamers	
4.1 Preface	62
4.2 Introduction	62
4.3 Results and Discussion	63
4.4 Concluding Remarks	70
Chapter 5: Future Work	72
Bibliography	73



## **List of Tables**

Table 4.3.1 Stability Analysis of cocaine-binding stem one variant aptamers

Table 3.3.1 Glumod-7 Normalized Signal Statistics

Table 3.3.2 Glumod-8 Normalized Signal Statistics

## List of Figures

Figure 1.1 Basic Diagram of SELEX

Figure 1.2 A non-exhaustive list of two nucleotide base pairs

Figure 1.3 Basic Diagram of Electrochemical Aptamer Based Sensor

Figure 1.4 Secondary structure and sequence of the originally selected cocaine-binding aptamer, MNS4.1.

Figure 1.5. Binding mechanism proposed for the MNS4.1 aptamer

Figure 1.6. Secondary Structure of Cocaine-binding Aptamers.

Figure 1.7 Secondary Structure of Cocaine-binding aptamer MN4

Figure 1.8 Secondary Structures of Cocaine-Binding stem one variant aptamers

Figure 1.9 Secondary Structure of Glucose-1 binding aptamer

Figure 1.10 Secondary Structure of Glucose modified binding aptamers

Figure 1.11 Basic Diagram of DSC

Figure 1.12 1D  $^1\text{H}$  NMR spectrum of a DNA glucose-binding aptamer to glucose with an inset focused on the imino region.

Figure 3.2.1. Secondary Structures of studied mono- and disaccharides.

Figure 3.3.1 Titration of Glumod-1

Figure 3.3.2 Titration of Glumod-2

Figure 3.3.3 Titration of Glumod-3 with Glucose

Figure 3.3.4 Titration of Glumod-4 with Glucose

Figure 3.3.5 Titration of Glumod-5 with Glucose

Figure 3.3.6 Titration of Glumod-6 with Glucose

Figure 3.3.7 Titration of Glumod-7 with Glucose

Figure 3.3.8 Titration curve of Glumod-7

Figure 3.3.9 Titration of Glumod-8 with Glucose

Figure 3.3.10 Titration curve of Glumod-8

Figure 3.3.11 Titration of Glumod-9 with Glucose

Figure 3.3.12 Titration of Glumod-10 with Glucose

Figure 3.3.13 Titration of Glumod-11 with Glucose

Figure 3.3.14 Titration of Glumod-12 with Glucose

Figure 3.3.15 Further Titrations of Glumod-12 with Glucose

Figure 3.3.16 Titrations of Glumod-13 with Glucose

Figure 3.3.17 Secondary Structures of Free State Glucose-Binding Aptamer Modifications

Figure 4.3.1 Analyzed Thermograms of Stem One Cocaine-binding Aptamer Variants

Figure 4.3.2 Gibbs Free Energy unfolding of stem one variants of cocaine-binding aptamers

## List of Abbreviations

$\Delta G$	Change in Gibbs Free Energy
$\Delta H$	Change in Enthalpy
$\Delta S$	Change in Entropy
DNA	Deoxyribonucleic Acid
ITC	Isothermal Titration Calorimetry
$K_d$	Dissociation Constant
mRNA	Messenger-RNA
NMR	Nuclear Magnetic Resonance
PCR	Polymerase-Chain Reaction
RNA	Ribonucleic Acid
SELEX	Systematic Evolution of Ligands by Exponential Enrichment
DSC	Differential Scanning Calorimetry
3D	Three Dimensional
A	Adenine
G	Guanine
T	Thymine
C	Cysteine
VEGF	Vascular Endothelial Growth Factor
E-AB	Electrochemical Aptamer Based
MB	Methylene blue
MW	Molecular Weight
UV	Ultraviolet

DMSO	Dimethyl sulfoxide
IDT	Integrated DNA Technologies
TEC	Thermal expansion coefficient
AP	2-aminopurine (AP)
2D	Two Dimensional
NOESY	Nuclear Overhauser Effect Spectroscopy
$T_m$	Melt Temperature
$C_p$	Heat Capacity
VWB	Very Weak Binding

# Chapter 1. Background and Introduction

## *1.1 Introduction to aptamers*

DNA encodes the instructions for life within segments of its primary sequence. Aptamers are distinguishable from other classes of nucleotides due to their capacity to form complex structures. This allows for their interaction with specific target molecules with incredible specificity and affinity<sup>1</sup>. Generally, aptamers are short single stranded DNA or RNA molecules which fold into three dimensional structures with or without the ligand present. They can be selected for a large variety of targets such as small molecules, ions, enzymes, and proteins employing all kinds of non-covalent interactions to bind their ligand<sup>2</sup>.

There are observed differences between DNA and RNA aptamers despite their similar nucleic acid structures. DNA aptamers are typically more stable in terms of chemical degradation and thermostability than their RNA counterparts due to their deoxyribose sugars<sup>3</sup>. Meanwhile, the chemical instability of RNA aptamers is primarily due to the 2' hydroxyl group on their ribose sugar which is more susceptible to a nucleophilic attack causing the breakage of a phosphodiester bond.<sup>4,5,6</sup> Typically, these aptamers require further chemical modifications during the initial oligonucleotide libraries or during the amplification stage of SELEX. These modifications are typically made at the 2'-position of their pyrimidine bases<sup>8</sup>. Examples of such modifications include methylation, formation of ethers, fluorination,<sup>9</sup> etc. These modifications applied to RNA molecules can make them as stable as DNA aptamers<sup>10</sup>. Furthermore, RNA aptamers occur in

nature as part of riboswitches<sup>11</sup>. Riboswitches are found in the untranslated region (UTR) of messenger RNA and are involved in gene regulation.

In 1990, Systematic Evolution of Ligands by Exponential Enrichment (SELEX) was developed independently by two research groups. Tuerk and Gold were originally trying to use an RNA sequence that could bind to T4 DNA polymerase<sup>12</sup>. Meanwhile, Ellington and Szotak were using a process to develop RNA sequences that bound to organic dyes<sup>13</sup>. Their results in time led to the developmental process that isolates ligand-binding aptamers from a randomized library of sequences known as SELEX.

## ***1.2 SELEX***

Systematic Evolution of Ligands by Exponential Enrichment or SELEX is an *in vitro* process in which aptamer candidates are screened and characterized in terms of binding affinity and specificity<sup>14</sup>. SELEX is made up of three main stages: selection, partitioning, and amplification. During the selection process, a large  $10^{15}$  oligonucleotide library of unique sequences, made up of two known sequence regions at the 5' and 3' ends, which surround a random region, is incubated with a specific target molecule<sup>12</sup>. Meanwhile, the partitioning phase keeps the sequences that bind to the target molecule and discards those that did not bind. Lastly, the amplification step is where numerous copies of the successfully bound candidate aptamers are made using Polymerase Chain Reaction (PCR). Typically, these steps are repeated numerous times with varying conditions to ensure optimal binding properties. A general overview of the SELEX process can be seen in figure 1.1.

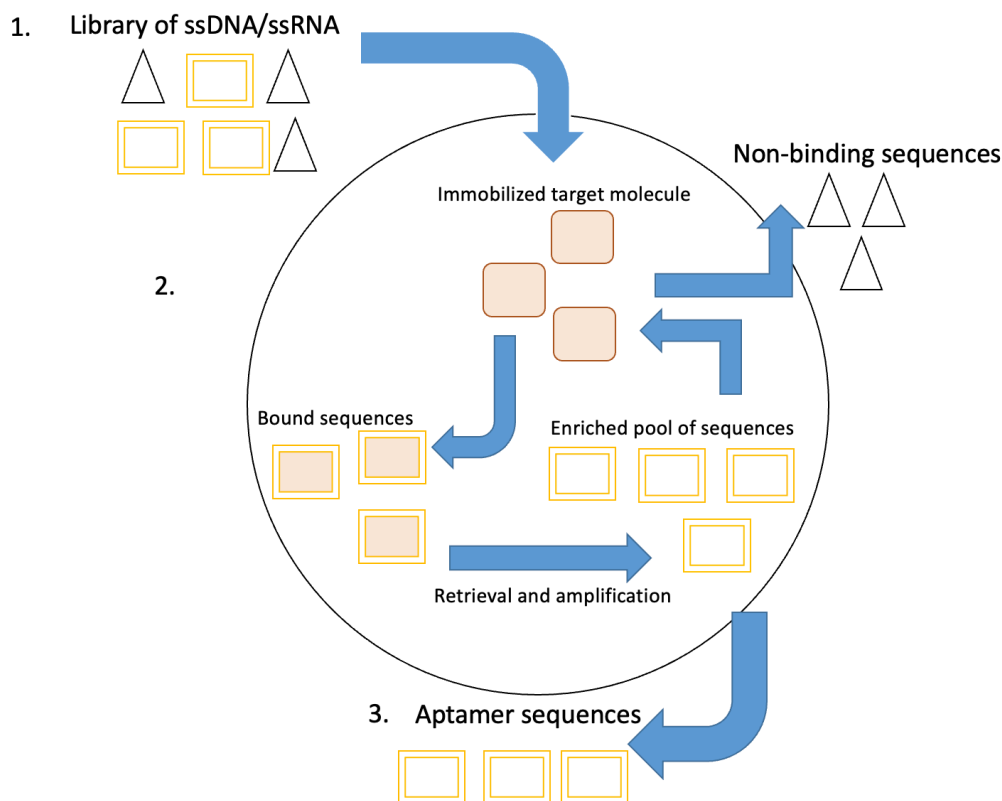


Figure 1.1: Basic Diagram of SELEX. **1.** The initial library is exposed to the ligand of interest. **2.** Bound sequences are retrieved, amplified and re-exposed to the ligand of interest while non-binding sequences are discarded. This step is repeated several times. **3.** After the cycles have ended, a set of aptamers with the desired characteristics are collected and sequenced.

### 1.3 Aptamer structure

The primary sequence of nucleic acids carries the instructions for their 3-dimensional structure and their functions. This structure plays a pivotal role in the specific binding between a ligand and an aptamer<sup>15,16</sup>. DNA will fold to maximize its stability by increasing the number of hydrogen bonds and van der Waals forces present resulting in a decrease of the entropy of the molecule<sup>17</sup>. An important structural component of DNA aptamers is the hydrogen bonding between complementary nitrogenous bases. These nitrogenous bases consist of two purines:

Adenine (A), Guanine (G), and two pyrimidines: Cytosine (C), and Thymine (T). The helical DNA structure is often a result of Watson-Crick A-T and C-G base pairing between the edges of the bases seen in figure 1.2. A helix's core is composed of stacked base pairs with the edges of the nitrogenous bases exposed in the major and minor grooves while the highly negative sugar-phosphate backbone is arranged around the exterior of the helix<sup>18</sup>.

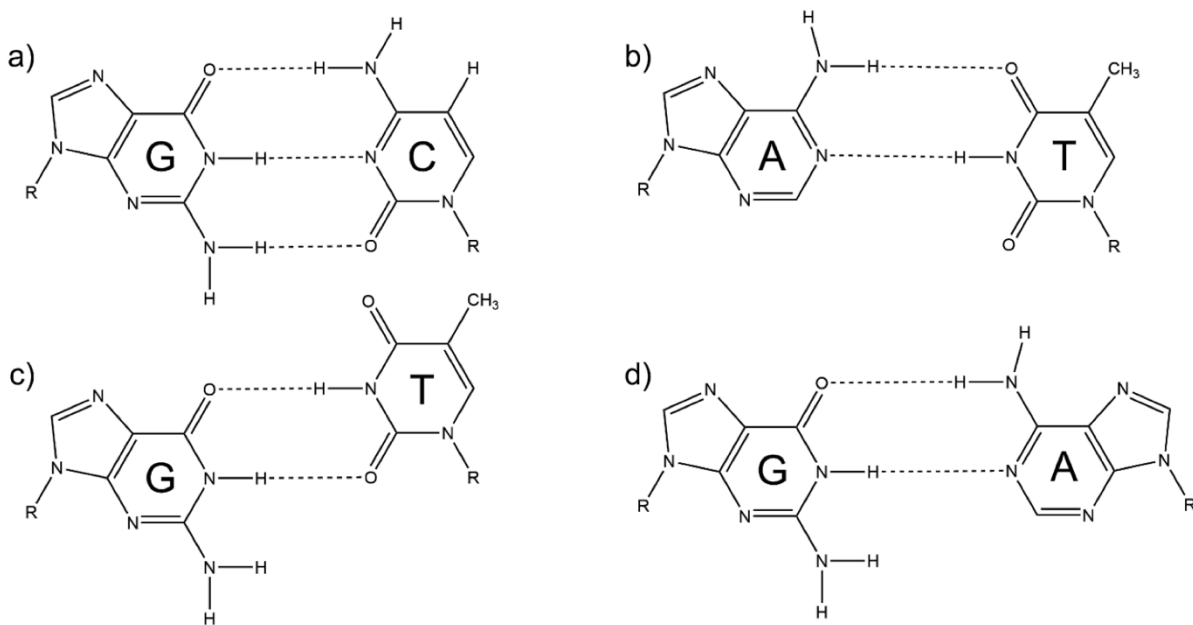


Figure 1.2 A non-exhaustive list of two nucleotide base pairs. Watson-Crick base pairs: **A.** Guanine-Cytosine; **B.** Adenine-Thymine; Non-Watson-Crick base pairs: **C.** Guanine-Thymine; **D.** Guanine-Guanine. Bases marked with a G are Guanine; A are Adenine; C are Cytosine; T are Thymine. Dashed lines represent hydrogen bonds between the various bases. This is a non-exhaustive list, there are other options for Non-Watson-Crick base pairs.

## ***1.4 Aptamer Applications***

Aptamers can be conducive to a vast array of applications due to their unique properties. Once SELEX was developed (See section 1.2) the aptamer field gained more research interest. Fields such as microbiology, medicine, and analytical chemistry became interested in their utilization. Aptamers can behave in various ways by interacting directly with a target, acting as a sensor for a drug targeted molecule, or in a diagnostic role. In 1998, the Macugen aptamer was the first to be used as a therapeutic to treat age related macular degeneration<sup>19</sup>. Macugen binds to the vascular endothelial growth factor (VEGF) that is responsible for leakages from vessels in the eye, which leads to its degradation, and the creation of new blood vessels in the eye. Macugen is an anti-VEGF aptamer and therefore binds to the target molecule preventing its function. Meanwhile, companies such as Pfizer are developing aptamer-based therapies for illnesses such as type 2 diabetes, heart disease, and leukemia<sup>20,21</sup>.

The clinical interest for aptamers is a result of their use in scenarios where traditional antibody-based therapies have not proven useful. Some of the advantages aptamers have in comparison to antibodies are the cost of development, accessible production, and reliable batch-to-batch reproducibility, as well as being able to be selected for a large variety of target molecules<sup>22,23</sup>. Additionally, aptamers are easily chemically modified such as the addition or modification of base pairs, addition of fluorescent tags, etc. thereby limiting enzymatic degradation in physiological conditions<sup>24</sup>. Meanwhile, the development of traditional antibodies is labor-intensive and time consuming with low batch-to-batch reproducibility<sup>22,23</sup>.

A common utilization of aptamers is in detection-based assays such as biosensors including optical sensors, molecular-mass-dependent sensors, or electrochemical sensors. Mass sensors can detect miniscule, small molecule mass changes and generate typically weak signals. While optical

sensors tend to give off a color change in the sensor when a binding event occurs between an aptamer and its ligand. For electrochemical sensors, a selected aptamer is immobilized on the surface of an electrode and the binding of the target ligand elicits a detectable electrochemical change in the system. In 2005, the E-AB sensor method was introduced by Plaxco et al. with the goal of being inexpensive, insensitive to its surrounding environment, and stable<sup>25</sup>. This research group used a previously selected aptamer<sup>26</sup> against the blood clotting enzyme thrombin, where ligand-induced conformational changes generate signals. E-AB sensors use the structure switching mechanism of nucleic acid aptamers or a redox reporter-ligand competition mechanism, which can be transduced into a measurable signal<sup>27</sup>.

E-AB sensors are made by covalently attaching a methylene blue (MB) labeled DNA aptamer to a gold electrode<sup>28</sup> seen in figure 1.3. For the structure switching mechanism of DNA aptamers, in the absence of the ligand, electron transfer between MB and the electrode is inhibited. In the presence of the ligand, the immobilized aptamer is presumably undergoing structural changes which allows for the MB to interact with the electrode more rapidly and transfer an electron. Another mechanism in which E-AB sensors use to operate is a redox reporter-ligand competition mechanism. This mechanism works as MB is covalently linked at the 3' end of the aptamer in the free state of the aptamer close to or at the binding site of the ligand, which causes the slow exchange of the electron. In the presence of the ligand, the aptamer undergoes conformational changes which displaces the MB closer to the surface of the electrode allowing for a faster exchange of an electron.

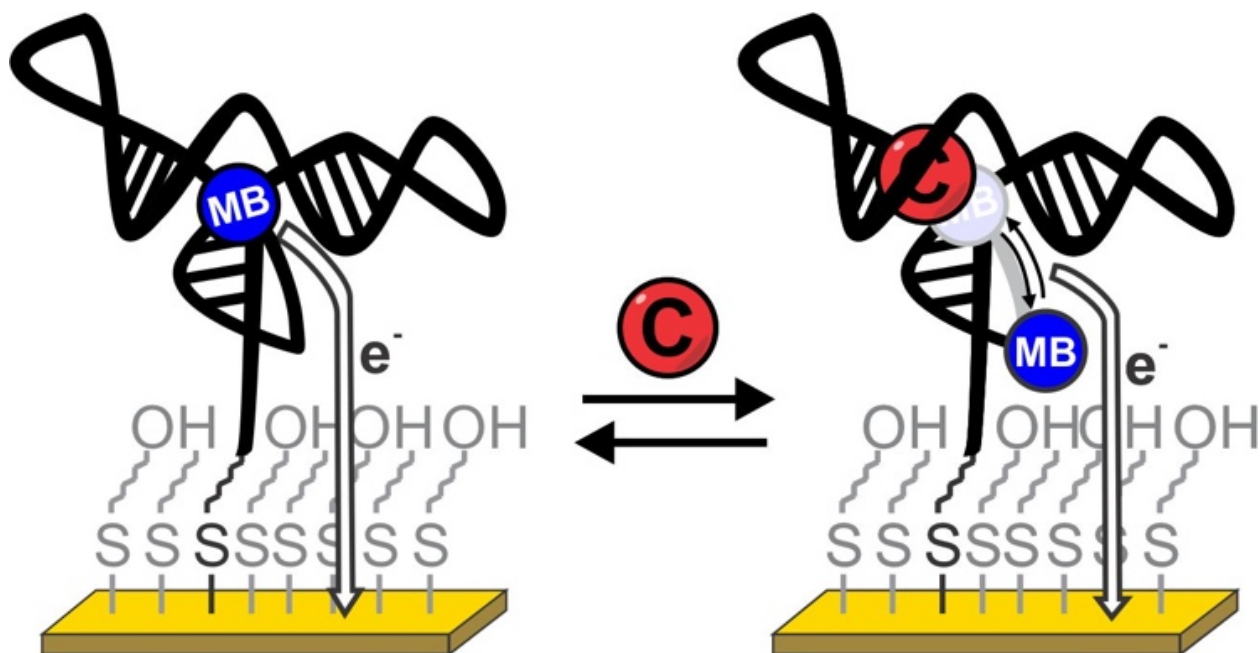


Figure 1.3. Basic Diagram of Electrochemical Aptamer Based Sensor. E-AB sensors are made by the covalent attachment of a MB labeled DNA aptamer to a gold electrode. Demonstrated above is the redox reporter-ligand competition mechanism which works by the covalent linkage of MB to the 3' end of the aptamer. The MB tag binds near or at the binding site of the ligand resulting in a slow electron transfer to the gold electrode. The MB molecule is then displaced in the presence of the ligand due to conformational changes allowing for a quicker electron transfer to the gold electrode. Image from Dauphin-Ducharme et al. 2023<sup>27</sup>.

### ***1.5 The Cocaine Binding Aptamer***

The cocaine-binding aptamer series is distinct as it is composed of three stems centered around a three-way junction. In 2000, Stojanovic et al. selected the parent cocaine-binding aptamer MNS4.1 with a high affinity for cocaine and a low affinity for its metabolites<sup>29</sup>. It is a 38-nucleotide aptamer with 5 non-canonical base pairs, stem one has 3 GA base pairs and stem three has GA and

GT base pairs. The secondary structure of MNS4.1 was predicted using mutation analysis including random and site-specific mutagenesis<sup>29</sup>. The predicted secondary structure can be seen in figure 1.4. It was initially hypothesized that the aptamer had one or more stems unfolded in the free state and required the presence of cocaine to have all three stems folded<sup>30</sup> seen in figure 1.5.

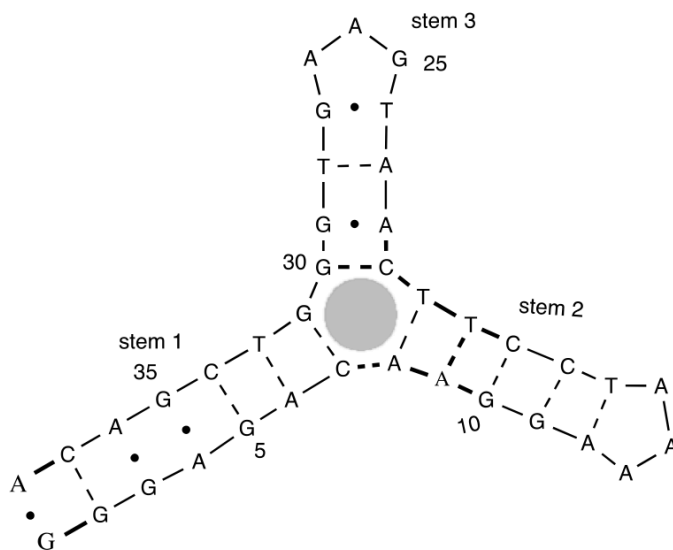


Figure 1.4 Secondary structure and sequence of the originally selected cocaine-binding aptamer, MNS4.1. The bound state is shown where the shaded circle is cocaine, the ligand. The dashed lines represent Watson-Crick base pairs, and the dots represent non-canonical base pairs. Image adapted from reference 29<sup>29</sup>.

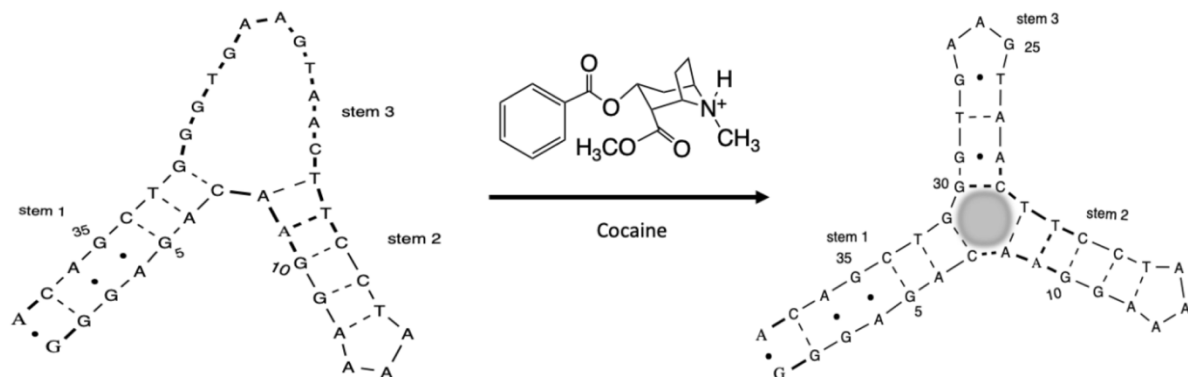


Figure 1.5. Binding mechanism proposed for the MNS4.1 aptamer. Stems 1 and 2 are completely folded shown in the free state on the left while on the right demonstrates the bound state and how stem 3 folds upon ligand binding. The shaded circle indicates the binding site for cocaine. Image adapted from reference 29<sup>29</sup>.

In 2014, a more recent study used a variant of the parent aptamer MNS4.1 named 38-GC. The goal of this study was to generate a fluorescence-based sensor which was able to detect cocaine in biofluids for example urine-based solutions<sup>31</sup>. In their study, 38-GC binds a fluorescent dye at the binding site of cocaine. In the presence of cocaine, the dye is displaced from the binding site therefore the fluorescent signal is observed.

The cocaine-binding aptamer is a widely used model system due to its ability to be manipulated to a preformed or structure-switching mechanism dependent on the number of base pairs in stem one. This manipulation is achieved by either dividing the aptamer into separate strands or by shortening the length of stem one to three or less base pairs<sup>32</sup>. The binding mechanism of the cocaine-binding aptamer was studied in 2010 by Neves et al. using ITC and NMR<sup>32</sup>. Their study determined that when stem one is three base pairs or less in a cocaine-binding aptamer that

it undergoes a structural change from an unstructured free state with minimal secondary structure to a bound state with a well-defined structure. Though if the aptamer's stem one is three base pairs or longer the free state is well-structured and there is very little structural change observed in the bound form.

The binding affinity is another well-studied aspect of the cocaine-binding aptamer series. In 2010, a study by Neves et al. examined the binding affinity of the MN series as a function of pH, stem length, and salt concentration<sup>33</sup>. They determined that lowering the pH resulted in decreasing the affinity of the aptamer, increasing the pH destroyed binding, and the optimal pH is where the amine in the cocaine molecule is expected to be protonated at 7.4. With varying salt (NaCl) concentrations they determined that the binding process is enthalpically driven this is counterbalanced by unfavorable binding entropy<sup>33</sup>. Their NMR results demonstrated that with every salt addition, a change in the dynamics of the aptamer was seen as the linewidth of the NMR spectra increased. As the cocaine molecule is protonated at optimal binding conditions it can indicate there are ionic interactions involved in the aptamer's binding mechanism. This interaction is not solely responsible for cocaine binding but does play an important role. Their assumption is that the negative DNA phosphate backbone interacts with the positive charge on the amine group of the cocaine molecule<sup>33</sup>. In terms of the length of the three stems, shortening the stems reduced binding affinity while increasing the stem length leads to an increased ligand affinity.

The thermal stability of cocaine-binding aptamers is a less studied area of their properties. In 2010, a study performed by Neves et al. studied the thermal stability of cocaine-binding aptamers: MN1, MN4, MN6, and MN19 seen in figure 1.6. Their values were determined using NMR and UV-vis (at 260nm), where they found that the longer stem one aptamers MN1 and MN4 are more stable than aptamers with a shorter stem one MN6 and MN19.

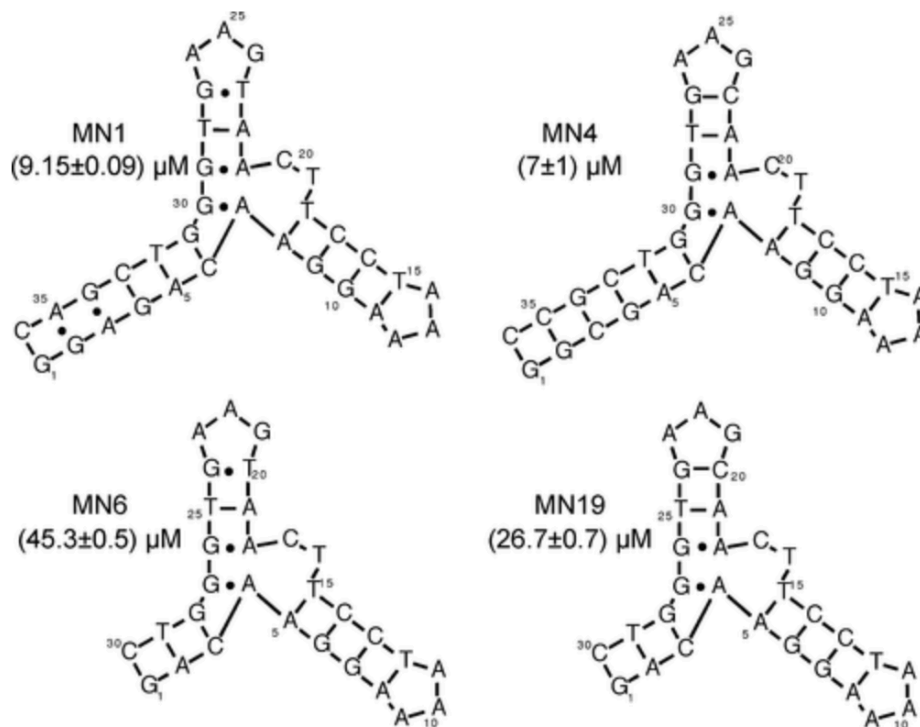


Figure 1.6 Secondary Structure of Cocaine-binding Aptamers. Adapted from reference 30.

Though originally selected to bind cocaine and not cocaine-metabolites, off-target ligand binding has been shown. In 2003, Stojanovic *et al.*, had a variant of their cocaine-binding aptamer which bound deoxycholic acid (DCA) and exhibited weak binding affinity to cocaine<sup>34</sup>. Furthermore, in 2009 it was demonstrated that this variant was able to bind quinine, an anti-malaria drug<sup>35</sup>. Additionally, it was discovered by Reinstein *et al.* that quinine bound to the cocaine-binding aptamer approximately 50 times stronger than cocaine, the original target ligand in SELEX<sup>36</sup>. In 2015, Slavkovic *et al.* examined the ability of cocaine binding aptamers to bind to 18 derivatives of quinine<sup>37</sup>, and later in 2018 investigated the binding ability to quinine based antimalarial compounds<sup>38</sup>.

One of the most studied variants of the cocaine-binding aptamer series studied by the Johnson Lab at York University is MN4 (figure 1.7) This aptamer consists of 36-nucleotides and was originally selected for cocaine ( $K_d= 5.5 \mu\text{M}$ ). Previous structural studies, show that MN4 is folded into a preformed structure which is thermodynamically favored; in the absence of cocaine<sup>33,39</sup>. Meanwhile, another well studied cocaine-binding aptamer, MN19 consisting of 30-nucleotides and has a structure switching mechanism where the free form does not have a fully formed stem one<sup>40</sup> and folds in the presence of the ligand. This is a common phenomenon in cocaine-binding aptamers where stem one has three or fewer base pairs such as the OR series (figure 1.8)

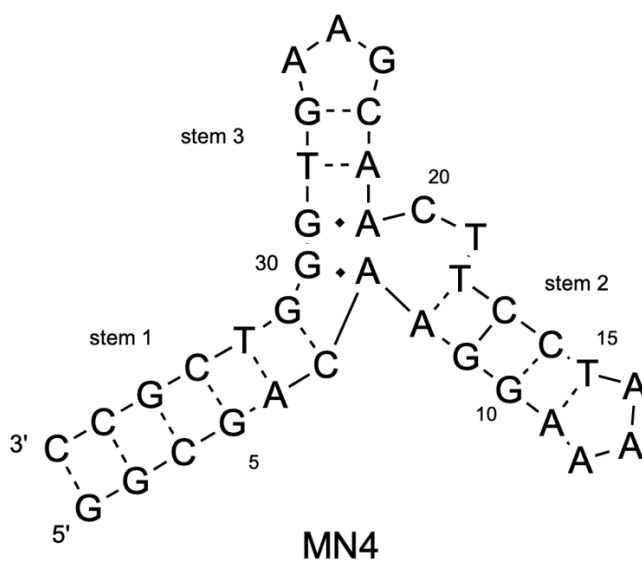


Figure 1.7 Secondary Structure of Cocaine-binding aptamer MN4. In the free-state MN4 is folded with little conformational changes upon binding.

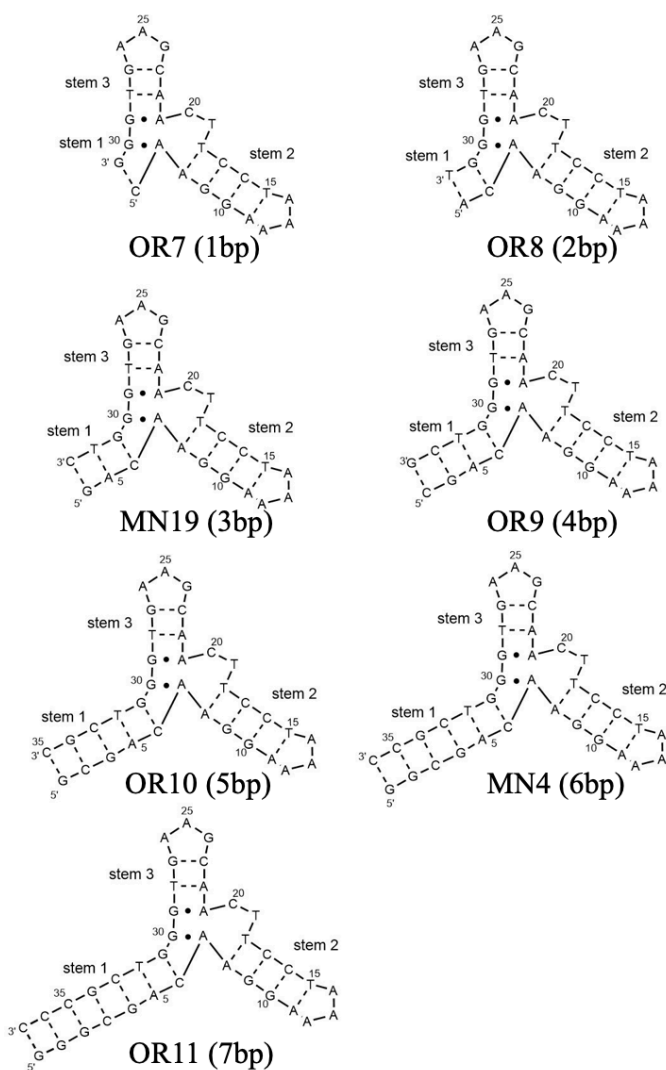


Figure 1.8 Secondary Structures of Cocaine-Binding aptamer stem one variant aptamers. The variants were created in the Johnson lab with the purpose of creating a more stable aptamer with a high affinity for quinine. The alterations made to this set of aptamers occurs in stem one with the elongation of the stem by one base pair with each additional aptamer, beginning at OR7 and finishing with OR11. These aptamers are shown in their folded-bound state. Image adapted from reference 41<sup>41</sup>.

## 1.6 The Glucose-Binding Aptamer

Recently, a glucose-binding aptamer was selected by the Stojanovic group denoted Glu-1<sup>42</sup>. Current glucose commercial biosensors rely heavily on enzymes. The primary issue with this is signal reduction either from chemicals present in the sample matrix or the rapid loss of enzyme activity<sup>16</sup>. Glucose has been considered a difficult target for aptamer selection and development as there is a moderate lack of chemical functionality variety for binding<sup>43</sup> as it is limited to hydroxyl groups.

Glu-1 is 40 nucleotides long and binds to glucose with a  $K_d$  of 10mM which poses a challenge for binding studies as comparable small molecule binding aptamers (the cocaine-binding aptamer) have greater affinities, in the low  $\mu$ M range (figure 1.8). Glu-1 can still be of physiological importance as blood glucose concentrations in the body typically range from 4mM-11mM<sup>15</sup>. Therefore, due to its weak affinity, titration studies using 1D Nuclear Magnetic Resonance (NMR) Spectroscopy were used due to its relative sensitivity in comparison to other methods. <sup>1</sup>H NMR spectroscopy was used to compare previously published data such as the affinity, specificity, and stability of the aptamer, and to try and develop an aptamer sequence variant with a greater affinity for glucose than the wild-type aptamer (Glu-1) that could be useful for future biosensing applications.

The secondary structure of Glu-1 was previously assigned by preliminary NMR studies by Zach Churcher at the Johnson Lab. As seen in figure 1.9 the free state is divided into different regions in relation to the central bulge in the free state of the aptamer. We originally hypothesized that binding would take place in the upper bulge region as with ligand binding the bulge is disjointed by two base pairs creating an upper and lower bulge region (figure 1.9). Therefore, the

first modification we made was to the lower bulge region to form Watson-Crick base pairs to increase the affinity of the aptamer by decreasing the free energy required to go into stabilizing the structure. Then we modified the hypothesized binding region to determine if it was the specific identity of the base that was important with binding or if it could be substituted with another purine/pyrimidine. For positive controls, we made modifications to the upper stem by changing a G-T base pair to a G-C base pair and changing the terminal triloop to a G-AA (figure 1.10). This approach of increasing the affinity of an aptamer by changing nucleic acids or base pairs is difficult and is seldomly done. We worked with this approach as we do not do SELEX and wanted to determine if it were possible to increase the affinity of the aptamer with singular nucleic acid modifications.

The goal of this project is to find a glucose binding aptamer with a greater affinity than Glu-1. Alterations have been made to the aptamer to determine where changes in the nucleotide sequence could be beneficial in terms of stability and affinity. The current modifications can be seen in Figure 1.10.

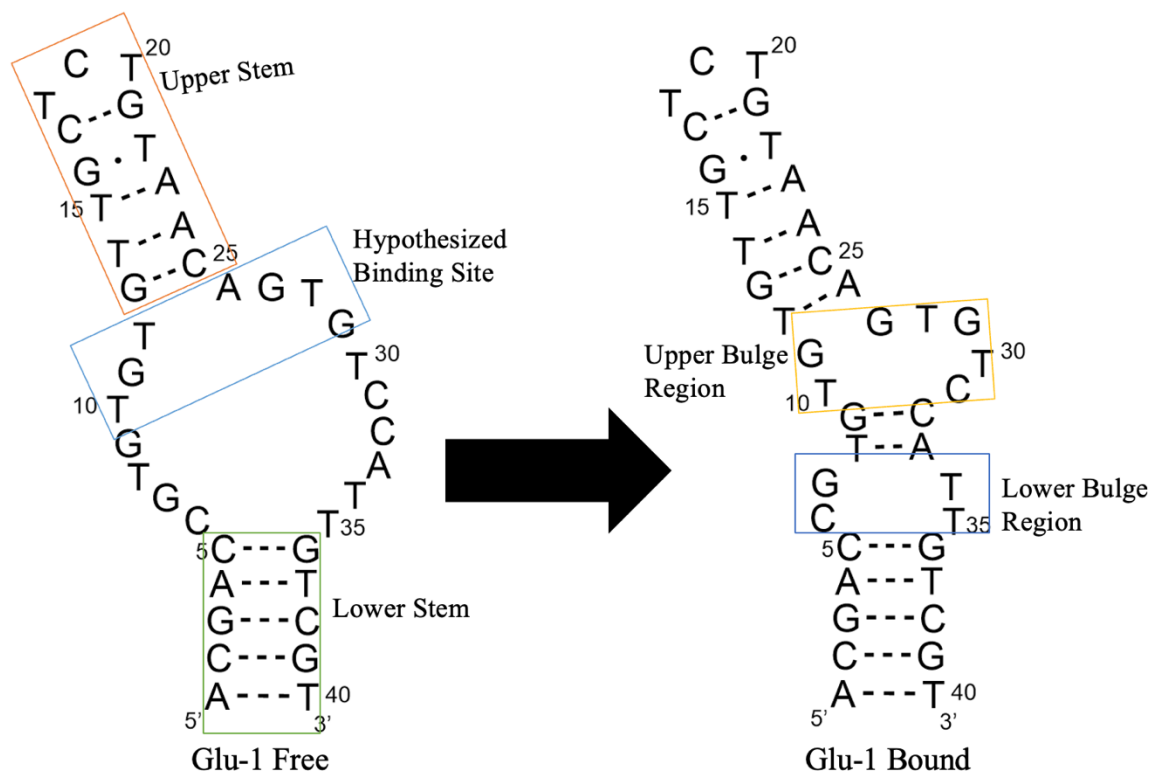


Figure 1.9 Secondary Structure of Glucose-1 binding aptamer bound to glucose. NMR assignments done by Zach Churcher.

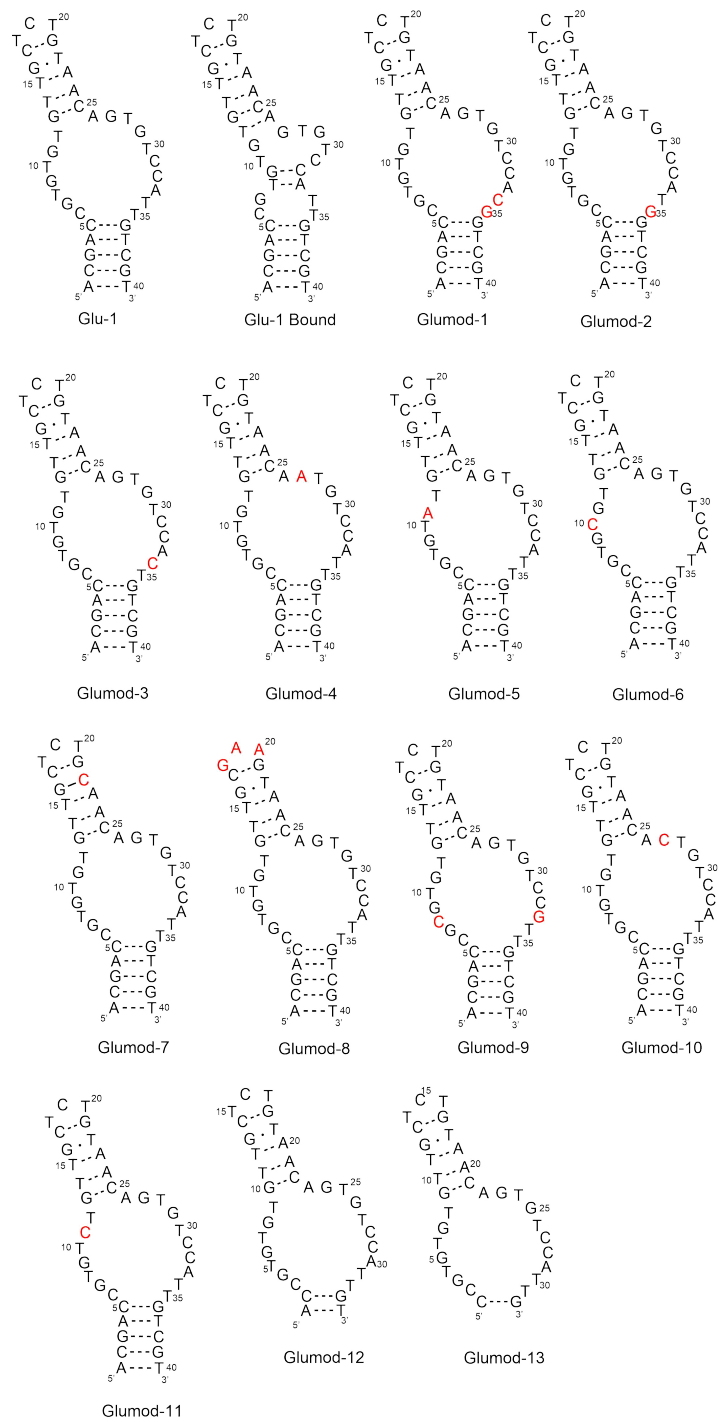


Figure 1.10 Secondary Structure of Glucose modified binding aptamers. These alterations were made to the glucose with the goal of finding an aptamer which bound with a higher affinity to the glucose molecule.

## 1.7 Differential Scanning Calorimetry

Differential scanning calorimetry (DSC) is a powerful biophysical tool with the purpose of identifying various thermal transitions and physical properties of polymeric materials as a function of temperature and time. As the temperature fluctuates, the heat quantity which is the heat emitted or absorbed by the sample is determined as the difference between the sample and reference cell measured by the instrument. It is assumed that the two cells are identical as they are contained within a common thermal enclosure as such the differential heat flow signal for the empty calorimeters is zero<sup>44</sup>.

There are two types of DSC based upon the mechanism of operation: heat-flux DSC and power compensated DSC. Heat-flux DSC has one furnace which encloses the thermoelectric disks where the sample pan and the empty reference pan are placed. The difference of temperature between the pans is measured by thermocouples and is converted to a heat flow signal<sup>44</sup>. However, power compensated DSC uses two separate furnaces one for the reference and one for the sample cells where both are maintained at the same temperature. The difference in thermal power required to keep them at the same temperature is plotted as a function of time thereby producing a thermogram (figure 1.11).

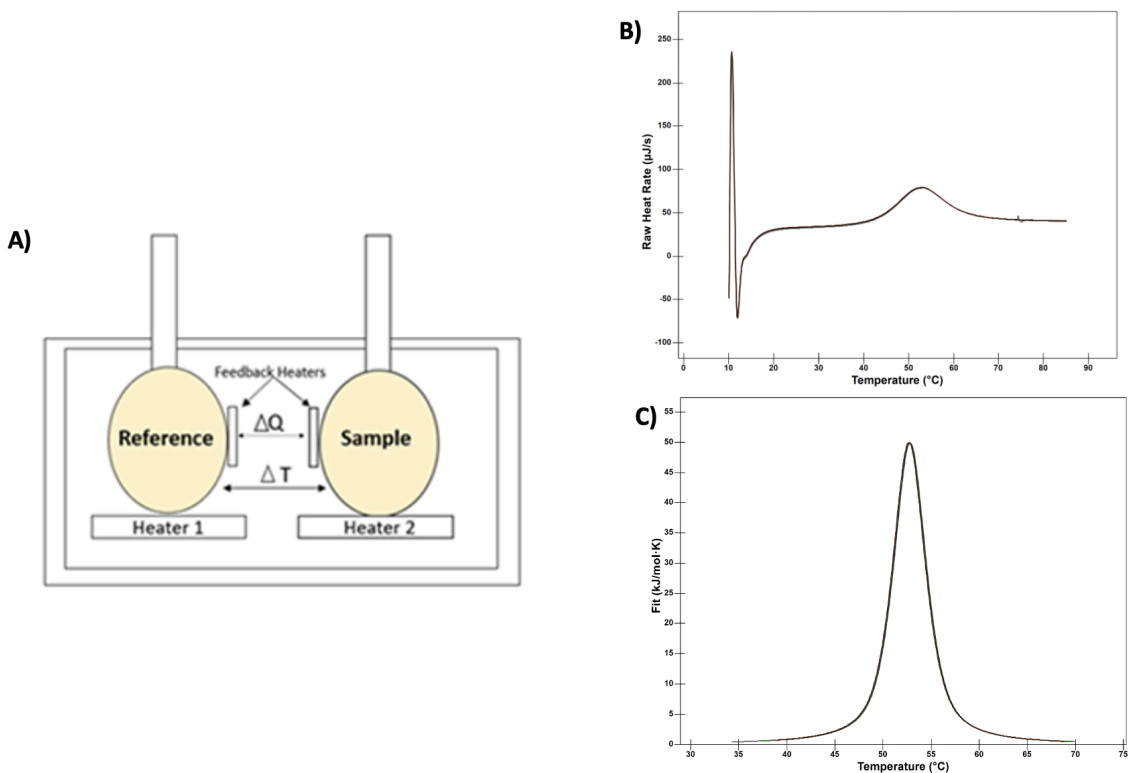


Figure 1.11 A) Diagram of a typical power compensated DSC instrument showing two cells (sample and reference), with their own heaters and feedback heaters. B) Sample DSC thermogram of an endothermic unfolding reaction. C) A sample sigmoidal fitted DSC thermogram of the unfolding event. By fitting the integrated curve to a suitable binding model (voight),  $\Delta H$  (area under the curve),  $\Delta G$ , and  $\Delta S$  can be determined.

The thermograms produced by power compensated DSC are used to extract thermodynamic parameters that govern the ligand binding and folding processes. A complete set of experiments includes 5 heating scans and 5 cooling scans. The benefit of using DSC is that it can be performed under near-physiological conditions and does not require labeling of the biomolecule or ligand. Though DSC does require the use of high temperatures (60°C-100°C) which can cause the denaturation or rearrangement of physiologically important ligands.

DSC can analyse a variety of molecules such as carbohydrates, nucleic acids, lipids, and proteins. In industry settings, DSC can be used to quantify the thermodynamic properties of various nano molecules. For example, DSC can be used to quantify pharmaceutical nanosolids, by determining the crystallinity percent of a sample with standards vs sample enthalpies<sup>45</sup>.

DSC is the most appropriate method to measure the thermodynamics of cocaine-binding aptamers. The high temperatures of the DSC do not negatively impact the sample as after each heat the aptamer will refold in the cooling scan and the scans can be run consecutively. DSC requires low concentrations of the aptamer typically ranging from 90-180 $\mu$ M (determined through experimental optimization), low volumes of 1mL per run and has a high throughput. Meanwhile, ITC would not be appropriate for answering my research questions as it measures binding affinity and not direct thermodynamic stability parameters, requires a large quantity of sample, and has a slow experimental time<sup>46</sup>. NMR is not ideal for these sets of experiments either as though it can measure thermodynamic properties such as entropy it does not give information regarding enthalpy, Gibbs free energy or heat capacity.

## **1.8 NMR Spectrometry**

With solution NMR spectroscopy, the sample containing the aptamer of interest is placed inside a strong magnetic field which enables the spin  $\frac{1}{2}$  nuclei present in nucleic acids to be studied. Depending on the chemical identity and local environment the nuclei will resonate at a characteristic frequency. Multiple experiments can be performed on the same sample under various conditions such as temperature, different buffer compositions, and the amount of the ligand present in the sample.

The resonances which belong to the imino protons of aptamers are studied in this project. The imino protons are quite useful as their signals are located downfield (at higher ppm values), from the rest of the signals found in nucleic acids such as the other protons on the nucleotide bases, and the protons found on deoxyribose sugars (figure 1.12). The chemical identity and surrounding environment dictate the position of an imino proton signal in an NMR spectrum<sup>40</sup>. The most downfield imino protons are those in Watson-Crick base pairs, showing up around 12-14 ppm with guanine iminos around 12-13 ppm and iminos from thymine or uracil around 13-14 ppm. Up field of the Watson-crick base pairs are non-Watson-Crick base pairs typically found in the 10-12 ppm range<sup>40</sup>.

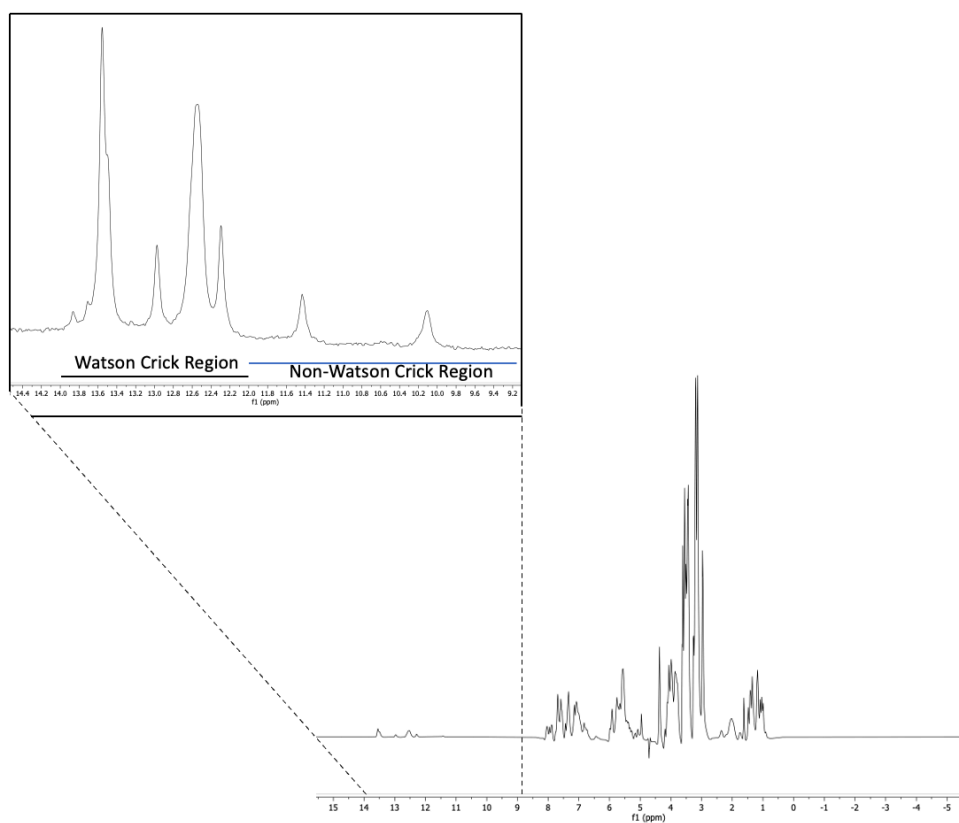


Figure 1.12 1D <sup>1</sup>H NMR spectrum of a DNA glucose-binding aptamer to glucose with an inset focused on the imino region.

## 1.9 Thesis Project

Previously published works have studied the pH, binding affinity, salt concentration, stem length, and limited thermodynamic properties of cocaine-binding aptamers. Therefore, the question remains about the thermodynamic stability properties of cocaine-binding aptamers with base pair modifications to stem one. Specifically in relation to structure-switching and preformed stem one aptamers and the changes to thermodynamics with ligand binding. The purpose of this project is to determine the stability of modified stem one aptamers with and without the ligand present using Differential Scanning Calorimetry (DSC). Additionally, it is of interest to determine the correlation if any of the free energy of binding to the designed increase of stability.

Current glucose sensing techniques lack long-term stability and the magnitude of output signals<sup>47</sup>. There remains a need to find a glucose aptamer which is stable long-term with a high affinity for glucose *in vivo*. Therefore, the goal of my project is to locate the binding site of the Stojanovic aptamer<sup>42</sup> Glu-1 aptamer, increase the binding affinity through base pair modifications in comparison to Glu-1 aptamer, and to better understand how the Glu-1 aptamer works.

## Chapter 2. Methods and Materials

### 2.1 Preface

This chapter includes methods used in subsequent chapters.

### 2.2 Aptamer Preparation

The aptamer samples acquired are from IDT as a lyophilized powder, then dissolved in ddH<sub>2</sub>O and exchanged 4 times against 2M NaCl then 4 times against ddH<sub>2</sub>O, using a 3 kDa concentrator. This was done to remove residual by-products that remained in the sample during the synthesis process. The concentrations of the aptamers were then determined by measuring the OD<sub>260</sub> in a UV-Vis spectrometer with the use of extinction coefficients provided by IDT.

### 2.3 Ligand Preparation

The ligand Quinine (C<sub>20</sub>H<sub>24</sub>N<sub>2</sub>O<sub>2</sub>) is acquired from Sigma-Aldrich as a powder, product number 145904. It is then weighed to achieve an excess of ligand in comparison to aptamer concentration near the maximum solubility of quinine (500mg/L)<sup>48</sup>. A minimum ratio used was 3:1 ligand to aptamer. Then quinine is dissolved in a phosphate buffer: 20mM sodium phosphate, 140mM NaCl, and 5mM KCl with a pH of 7.4.

### 2.4 DSC Equipment Setup

#### 2.4.1 General

The DSC buffer includes: 20mM sodium phosphate, 140mM NaCl, and 5mM KCl with a pH of 7.4. The buffer as well as the biomolecule are degassed using a thermovac unit twice on a 15-minute timer before being loaded into the DSC to avoid introducing bubbles in the machine.

Equilibration of the DSC with the working buffer is done by performing a forward (heating step) and a reverse (cooling step) scan. An aptamer is dissolved in working buffer described above then loaded into the sample cell. The reference cell is loaded with the same buffer as the sample

cell. To ensure the reproducibility and accuracy of the resulting thermograms 5 heating and 5 cooling scans are run. For the analysis of the results, the raw power data is exported as files in the DSC data analysis software Nanoanalyze<sup>17</sup>.

#### 2.4.2 Data Analysis

The analysis of the results is conducted using the Nanoanalyze software. For the melt of aptamers, each scan is analysed individually. The buffer-buffer run is used as a blank for each scan before they are fit to a sigmoidal baseline. Next the scans are applied to a Voight model where numerous iterations are applied before the final properties are extracted from a scan. The scans are then compiled onto one graph and the values are averaged to determine the thermodynamic properties. The thermodynamic properties given through the software are the melt temperature and the enthalpy. Further thermodynamic properties were determined using the equations below:

Binding Affinity

$$K_d = \Delta G_{bound} - \Delta G_{free}$$

Where  $K_d$  is the dissociation constant (binding affinity),  $\Delta G_{bound}$  is the Gibbs free energy of the bound sample,  $\Delta G_{free}$  is the Gibbs free energy of the free sample.

Gibbs Free Energy

$$\Delta G = \Delta H - T\Delta S$$

$$\Delta G = RT \ln K_d$$

Where  $\Delta G$  is Gibbs free energy,  $\Delta H$  is the enthalpy,  $T$  is the temperature at a certain point of the heat,  $\Delta S$  is the entropy, and  $R$  is the gas constant.

Entropy

$$\Delta S = \frac{\Delta H}{T}$$

Where  $\Delta S$  is the entropy,  $\Delta H$  is the enthalpy, and  $T$  is the temperature at a certain point of the heat.

## 2.5 <sup>1</sup>H NMR Equipment Setup and Analysis

1D NMR experiments were carried out on a 600 MHz Bruker Avance spectrometer. The water signal in the spectra was suppressed using excitation sculpting<sup>49</sup>. Excitation sculpting uses a low-power soft 180 degrees pulse which flips and retains all the resonances while the water peak is attenuated. Experiments involving glucose (Sigma Aldrich, product number G7021) were carried out in 250mM NaCl, 10mM H<sub>x</sub>Na<sub>y</sub>PO<sub>4</sub>, pH 7.6, 10% D<sub>2</sub>O, 5°C. We work at 5 °C to reduce the dynamics and the rate of exchange of the protons with the solvent. Glucose-binding aptamers with a concentration of 500μM were titrated with glucose and NMR experiments were run with concentrations of 0.5mM, 1mM, 2mM, 5mM, 10mM, 20mM and 40mM glucose in the aptamer sample. With the addition of glucose, 1D spectrum of the sample was acquired and compared to the free spectrum of the sample prior to the addition.

These spectra were processed, and figures were prepared using TOPSPIN 3.5 (Bruker). The affinity of the aptamer-glucose interaction was determined by rearranging the equation below<sup>50</sup>. The fraction bound ( $f_b$ ) was fit as a function of the glucose concentration using the equation below:

$$f_b = B_{max} \frac{[L]}{K_d + [L]}$$

Where  $B_{max}$  is the maximum response,  $K_d$  is the dissociation constant (binding affinity), and  $[L]$  is the concentration of glucose present in the NMR sample. The fraction bound at a certain point during the titration was calculated using the equation below:

$$f_{bi} = \frac{\delta_i - \delta_0}{\delta_f - \delta_0}$$

Where  $f_{bi}$  is the fraction bound at a specific point during the titration,  $\delta_i$  is the  $^1\text{H}$  position of a particular resonance,  $\delta_0$  is the initial  $^1\text{H}$  position of the resonance in the absence of glucose,  $\delta_f$  is the final  $^1\text{H}$  position of the resonance being studied. This calculation is under the assumption that the aptamer is fully bound with a  $f_{bi}$  of 1 at the final titration point. For these spectra the peak intensity was used instead of chemical shift, peak volume could have also been used. Nonlinear curves were fit using SigmaPlot.

## **Chapter 3. Affinity Analysis of Modified Glucose-Binding Aptamers**

### **3.1 Preface**

All the data presented in this chapter was acquired and analyzed by me however previous members in the lab have contributed to this research by conducting preliminary studies.

### **3.2 Introduction**

Previous studies by other labs with the Glu-1 aptamer were conducted using fluorescence methods due to the weak affinity of the aptamer<sup>43</sup>. The sole modification which was made previously to Glu-1 was the addition of 2-aminopurine (AP) probe which allowed for a quicker fluorescence signal change<sup>15</sup>. The research group determined the aptamers selectivity for glucose compared to other mono- and disaccharides (figure 3.2.1). Their results indicated that there was no binding with fructose and moderate binding was seen with galactose though it saturated at a lower fluorescence than glucose. Disaccharides sucrose and trehalose, bind with a  $>150\text{mM } K_d$ , though demonstrated comparable final fluorescence proposing they end at a final binding structure close to glucose. Though in blood, it's demonstrated that only glucose is readily available at high concentrations<sup>51</sup>. Therefore, the aptamer exhibits selectivity for glucose.

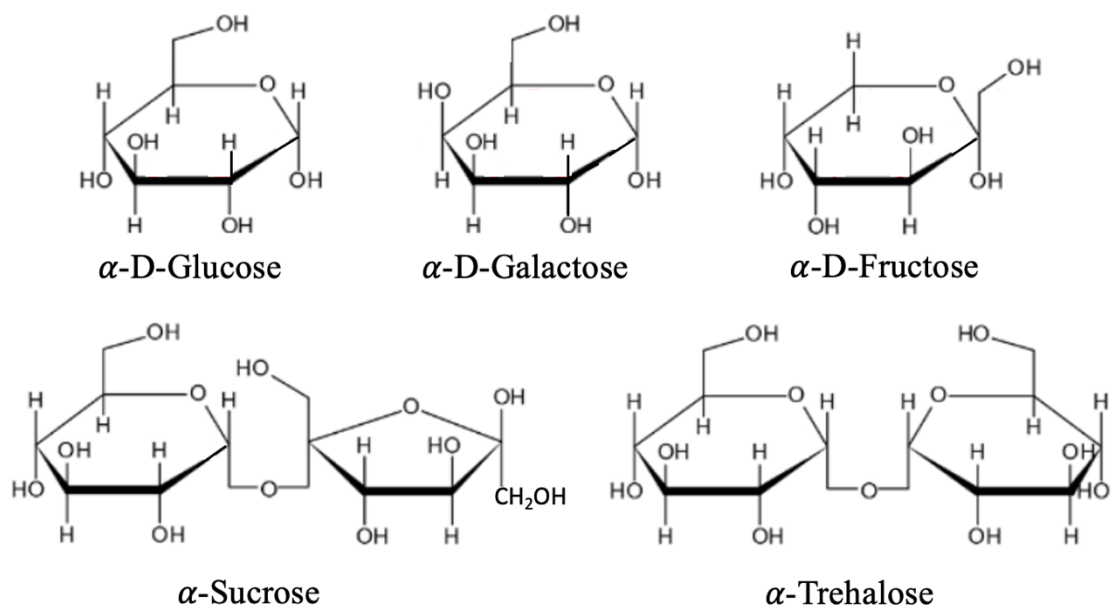


Figure 3.2.1. Secondary Structures of studied mono- and disaccharides.

Previous unpublished studies conducted by the Johnson lab aimed to determine the validity of these previously published results<sup>43</sup>. Firstly, the secondary structure was confirmed using a 2D NOESY for the glucose-bound and free state of the wild type Glu-1 aptamer where imino proton assignments were established. The binding affinity was then studied to ensure it falls within the physiological range of glucose. These experiments were done using 1D NMR titrations with glucose and the parent aptamer Glu-1. The  $K_d$  was determined to be 5mM through titration curve analysis of the intensity of imino proton peaks which was similar to the previously published  $K_d$  of 10mM. Furthermore, using 1D NMR experiments, Glu-1 was titrated with galactose to determine the aptamer's specificity to glucose where no off-target binding was observed as no new

imino proton peak signals were seen as well as no chemical shift changes in the spectra. The next step in the project was the designing of modifications to the base pairs in the Glu-1 aptamer.

The modified glucose binding aptamers are denoted as Glumod-#. Some of the modifications, Glumod-1, Glumod-2, Glumod-3, Glumod-7, Glumod-9, Glumod-10, Glumod-11 were made with the idea of forming additional Watson-Crick base pairs in the bound-state which would increase the stability of the free aptamer (figure 1.9). This was done as lessening the  $\Delta G$  of binding devoted to stabilizing the structure will result in an increase of the observed binding affinity<sup>52</sup>.

The first modification made was Glumod-1 where two non-Watson Crick base pairs were changed to form C6-G35 and G7-C36 respectively (figure 1.9). We believed this modification would increase the stability of the molecule and not interfere with binding as the hypothesized binding pocket involved the top region of the bulge nucleotides G11, T12, A26, G27, T28, G29 (figure 1.9). Glumod-2 (G35) and Glumod-3 (C34) separated the combined modifications of Glumod-1. Glumod-9 switched the positions of G9 and C32 to attempt to induce a Watson-Crick base pair. Glumod-10 changed base 26 to a C to attempt to induce a Watson-Crick base pair into the hypothesized binding region. Glumod-11 altered G11 to a C to attempt to induce a Watson-Crick base pair into the binding region (figure 1.9).

Glumod-4 was created to ensure the bases at the top of the bulge were vital for binding the glucose molecule (figure 1.9). The base G27 was changed to an A, to determine if the base could be a purine or if the G itself was important in binding. Glumod-5 altered G11 to an A to determine if this G was also crucial for binding of the glucose molecule. Glumod-6 switched T10 to C10 to determine if this was another important nucleotide in binding as it was originally just outside of where the binding pocket was believed to be (figure 1.9).

Glumod-7 was a positive control where a base further from the binding pocket was altered from a T22 to a C22 to attempt to induce a more stable Watson-Crick base pair thereby stabilizing the free structure. Furthermore, to attempt to confirm the upper stem region was not involved in binding. Glumod-8 was a positive control where the terminal triloop was changed to a GAA which is the most stable terminal triloop sequence.

Glumod-12 was truncated as it was believed that these residues do not play an important role in binding of the glucose molecule. Glumod-13 was a 4 base pair truncation to determine the importance of the bases further from the binding site. These modifications were studied using 1D NMR to determine if binding occurs.

### **3.3 Results and Discussion**

Glumod-1 (figure 3.3.1) was titrated from 0mM glucose to 20mM glucose though no new signals or chemical shift changes were seen in the imino proton region indicative of no binding present with subsequent additions of glucose. It was believed that two modifications at once could have resulted in the loss of binding. Therefore, these modifications required separation to determine which was the cause of this loss.

Glumod-2 (figure 3.3.2) was titrated from 0mM to 20mM glucose though no new signals or chemical shift changes were seen in the imino proton region indicative of no binding present with the subsequent additions of glucose. Therefore, we moved forward with the idea that this mutation from Glumod-1 was the cause of the loss of binding in the modification.

Glumod-3 (figure 3.3.4) was titrated from 0mM to 20mM glucose though no new signals or chemical shift changes were seen in the imino proton region indicative of no binding present with the subsequent additions of glucose. These results indicated that both modifications from

Glumod-1 caused the loss of binding of the aptamer. This led us to believe that the bases T35 and T34 and this smaller lower bulge played a role in the binding of glucose.

Glumod-4 (figure 3.3.5) was titrated from 0mM to 20mM glucose though no new signals or chemical shift changes were seen in the imino proton region indicative of no binding present with the subsequent additions of glucose. Indicating that the guanine at this position was important in the binding pocket and that it could not be substituted with another purine base.

Glumod-5 (figure 3.3.6) was titrated from 0mM to 20mM glucose though no new signals or chemical shift changes were seen in the imino proton region indicative of no binding present with the subsequent additions of glucose. Indicating that the guanine at this position was important in the binding pocket and that it could not be substituted with another purine base.

Glumod-6 (figure 3.3.7) was titrated from 0mM to 20mM glucose though no new signals or chemical shift changes were seen in the imino proton region indicative of no binding present with the subsequent additions of glucose. Though slightly outside of the hypothesized binding region T10 is an important nucleotide for binding and cannot be substituted with another pyrimidine base.

Glumod-7 (figure 3.3.8) was initially titrated from 0mM to 20mM glucose, new signals were seen in the imino proton region indicative of binding present with the subsequent additions of glucose. Therefore, it is indicative that the upper stem is more susceptible to nucleic acid changes than the center bulge or the nucleotides close to the hypothesized binding pocket (figure 1.9). With the presence of binding, more titrations were performed to create a titration curve with 13 points from 0mM to 80mM glucose (Figure 3.3.9). From the titration curve, a dissociation constant ( $K_d$ ) was calculated to be  $2.91\text{mM} \pm 0.3\text{mM}$  ( table 3.3.1). Though slightly smaller than

the parent aptamer Glu-1 it is not out of the error range of its  $K_d$   $5\text{mM} \pm 2\text{mM}$ . Therefore, this modification is not significantly different in terms of affinity to glucose than the parent aptamer Glu-1.

Glumod-8 (figure 3.3.10) was initially titrated from 0mM to 20mM glucose, new signals were seen in the imino proton region indicative of binding present with the subsequent additions of glucose. Therefore, further supporting that the upper stem is more susceptible to change than the center bulge or the nucleotides close to the hypothesized binding pocket. With the presence of binding, more titrations were performed to create a titration curve with 13 points from 0mM to 80mM glucose (figure 3.3.11). From the titration curve, a dissociation constant ( $K_d$ ) was calculated to be  $12\text{mM} \pm 3\text{mM}$  (table 3.3.2). Therefore, this modification significantly reduced the affinity of the aptamer to glucose. Hypothesized that this decrease is a result of the terminal triloop playing a role in long range interactions and by changing the nucleotides it resulted in a change in the dynamics of the stem.

Glumod-9 (figure 3.3.12) was titrated from 0mM to 20mM glucose though no new signals were seen in the imino proton region nor were chemical shift changes observed indicative of no binding present with the subsequent additions of glucose. Therefore, the positions of these bases are important to binding of the glucose molecule. Further affirming that the bases slightly outside of the hypothesized binding pocket play a role in the binding of the glucose molecule (figure 1.9).

Glumod-10 (figure 3.3.13) was titrated from 0mM to 20mM glucose though no new signals were seen in the imino proton region nor were chemical shift changes observed indicative of no binding present with the subsequent additions of glucose. Therefore, indicating that the bulge region is important in binding and that a base pair in the upper bulge region confines the flexibility of the bases which might play a role in binding.

Glumod-11 (figure 3.3.14) was titrated from 0mM to 20mM glucose though no new signals or chemical shift changes were seen in the imino proton region indicative of no binding present with the subsequent additions of glucose. Further supporting that the bulge region is important in binding and that a base pair in the upper bulge region confines the flexibility of the bases which might play a role in binding.

Glumod-12 (figure 3.3.15) was initially titrated from 0mM to 20mM glucose, new signals were seen in the imino proton region indicative of binding present with the subsequent additions of glucose. This was indicative that the lower stem did not play a role in the binding to glucose. With the presence of binding, more titrations were performed to create a titration curve with 13 points from 0mM to 80mM glucose (figure 3.3.16). Though when further titrations of this modification were done, it was seen from the NMR spectra that this aptamer would bind weaker than the parent aptamer therefore a titration curve was not extracted from the data as the affinity would not have been improved. The weaker binding was seen from the initial noisy baseline in figure 3.3.15, and then weaker signals were observed in figure 3.3.16. We believe this weaker binding is caused by the loss of stability as more  $\Delta G$  goes into folding the molecule therefore decreasing binding affinity.

Glumod-13 (figure 3.3.17) was titrated from 0mM to 20mM glucose though no new signals or chemical shift changes were seen in the imino proton region indicative of no binding present with the subsequent additions of glucose. Therefore, indicating for the aptamer to be functional it cannot have more than 3 base pairs truncated from the lower stem (figure 1.9).

In both this study and the previous study of the Glu-1 parent aptamer it is demonstrated that the binding pocket for the glucose molecule is larger than the top region of the central bulge

(figure 1.9). Furthermore, it demonstrated that the Glu-1 is highly specific to glucose and does not have off target binding to other disaccharides galactose and sucrose.

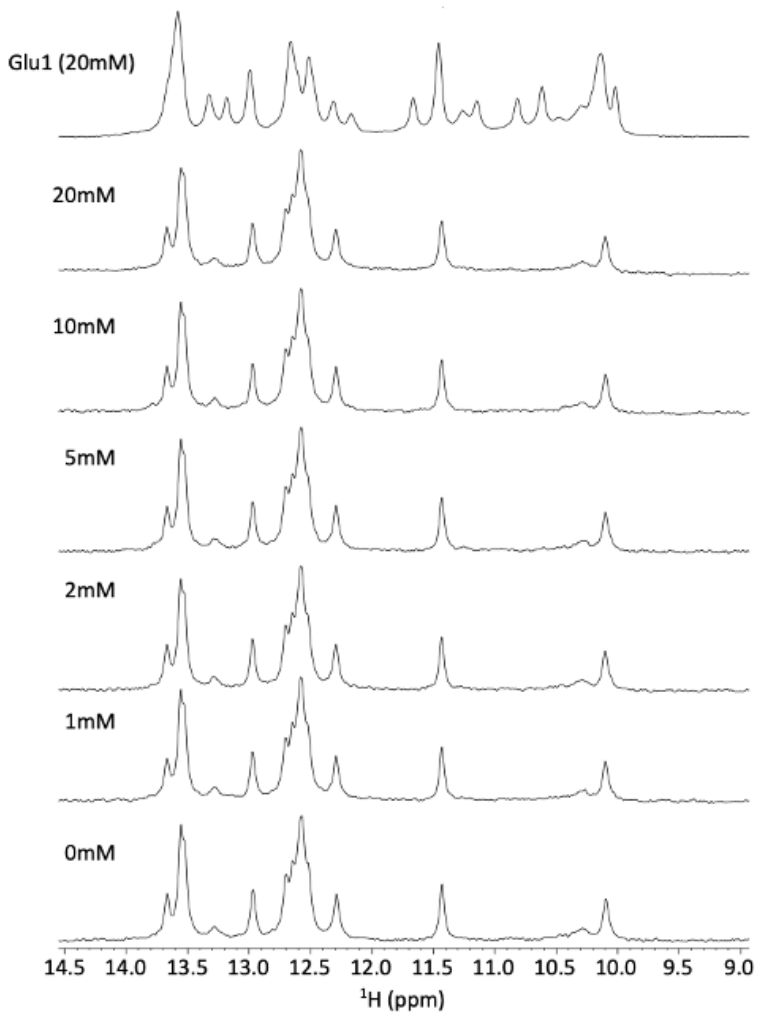


Figure 3.3.1 Titration of Glumod-1 with Glucose. With each addition of glucose, no new signals or chemical shift changes in imino peak region was observed therefore no binding was observed. Glumod-1 500mM, buffer conditions: 250mM NaCl, 10mM  $\text{H}_2\text{Na}_2\text{PO}_4$ , pH 7.6, 10%  $\text{D}_2\text{O}$ . Experiment performed by Zach Churcher.

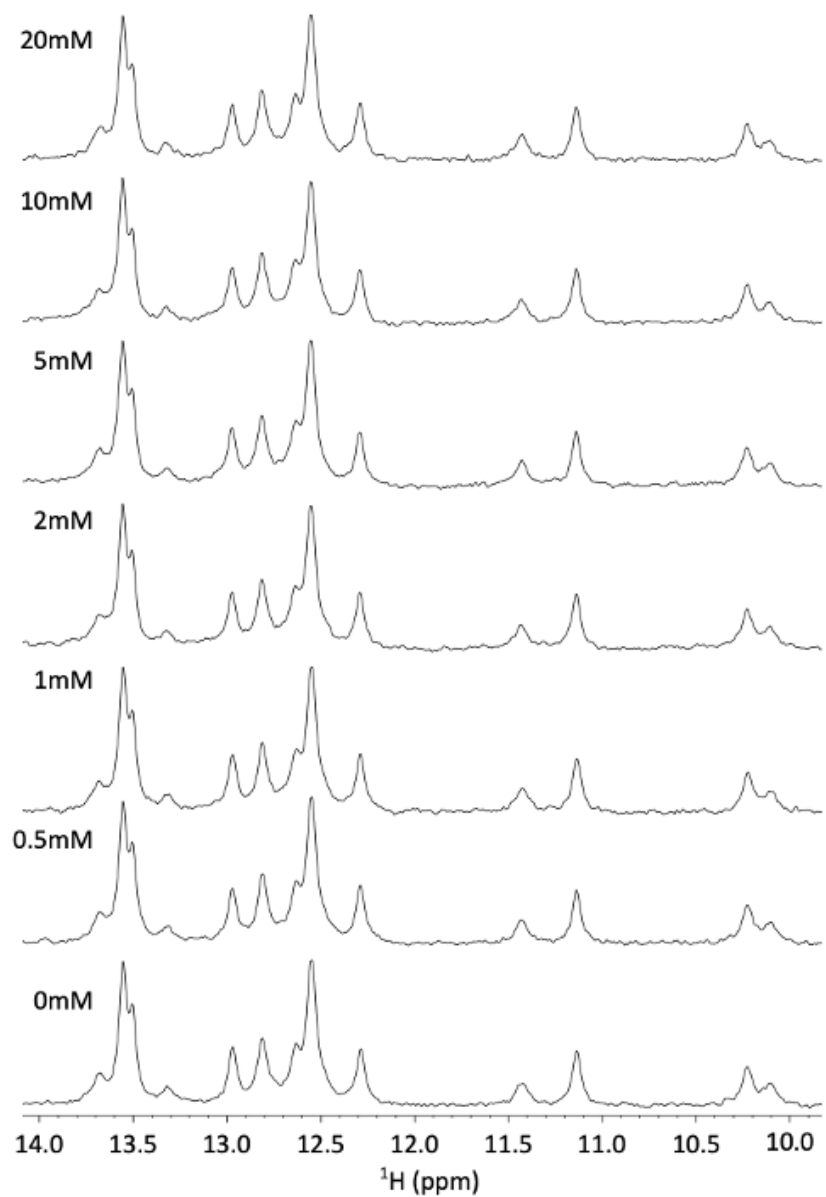


Figure 3.3.2 Titration of Glumod-2 with Glucose. With each addition of glucose, no new signals or chemical shift changes in imino peak region were observed therefore no binding was observed. Glumod-2 500mM, 250mM NaCl, 10mM  $\text{H}_2\text{N}_2\text{PO}_4$ , pH 7.6, 10%  $\text{D}_2\text{O}$ .

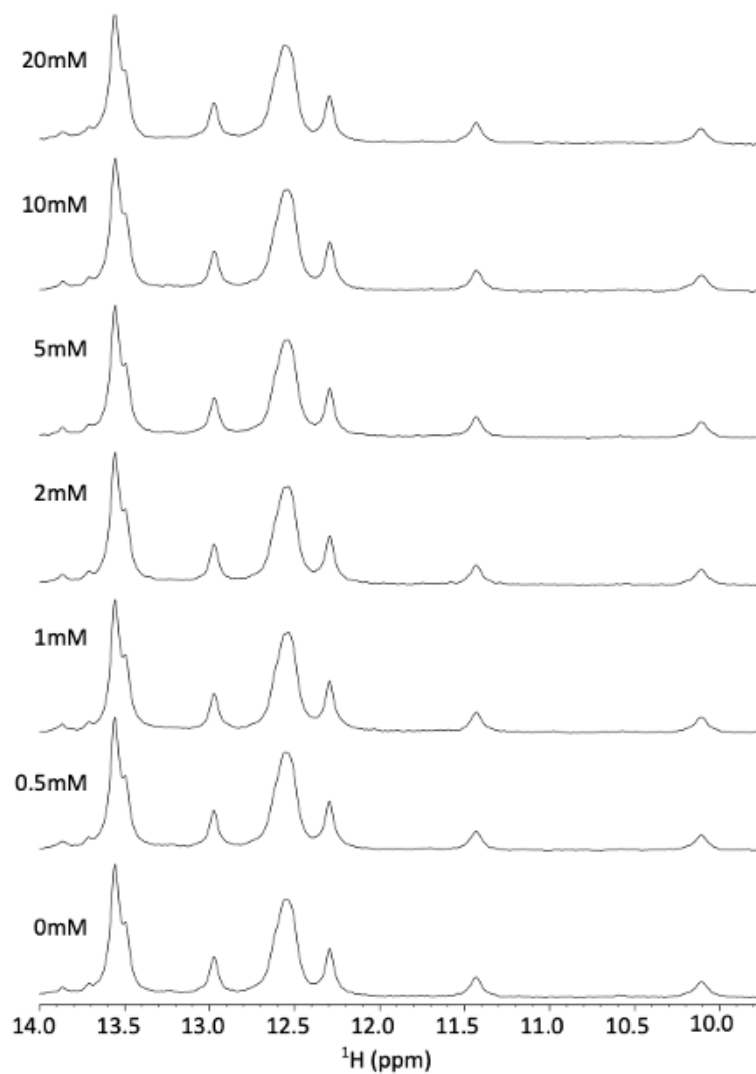


Figure 3.3.4 Titration of Glumod-3 with Glucose. With each addition of glucose, no new signals or chemical shift changes in imino peak region were observed therefore no binding was observed. Glumod-3 500mM, 250mM NaCl, 10mM  $\text{H}_2\text{N}_2\text{PO}_4$ , pH 7.6, 10%  $\text{D}_2\text{O}$ .

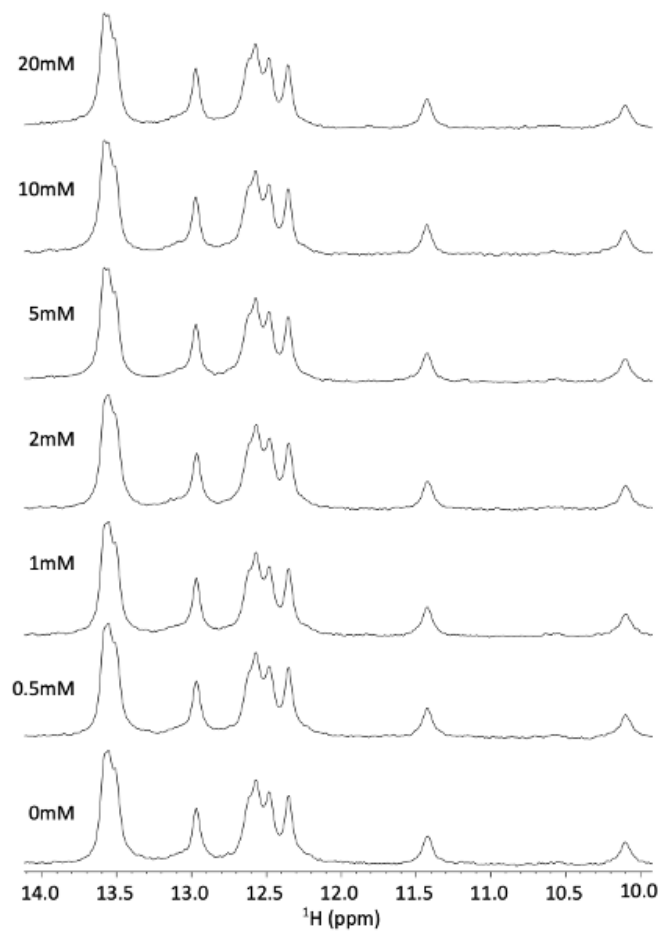


Figure 3.3.5 Titration of Glumod-4 with Glucose. With each addition of glucose, no new signals or chemical shift changes in imino peak region observed therefore no binding was observed. Glumod-4 500mM, buffer conditions: 250mM NaCl, 10mM  $\text{H}_2\text{Na}_2\text{PO}_4$ , pH 7.6, 10%  $\text{D}_2\text{O}$ .

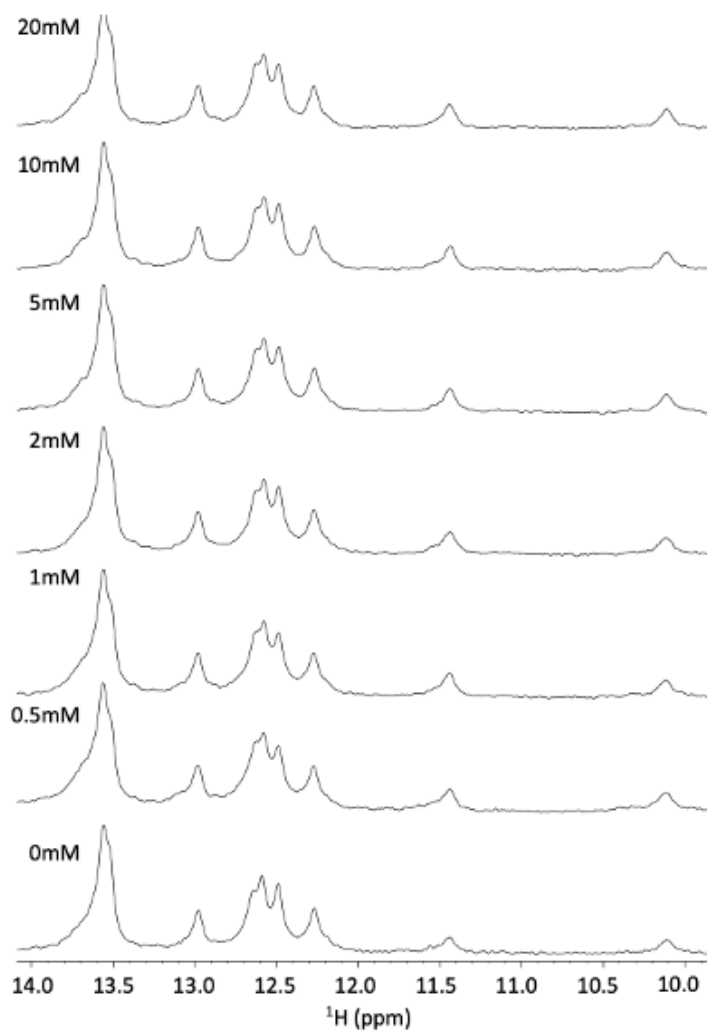


Figure 3.3.6 Titration of Glumod-5 with Glucose. With each addition of glucose, no new signals or chemical shift changes in imino peak region therefore no binding was observed. Glumod-5 500mM, buffer conditions: 250mM NaCl, 10mM  $\text{H}_2\text{Na}_2\text{PO}_4$ , pH 7.6, 10%  $\text{D}_2\text{O}$ .

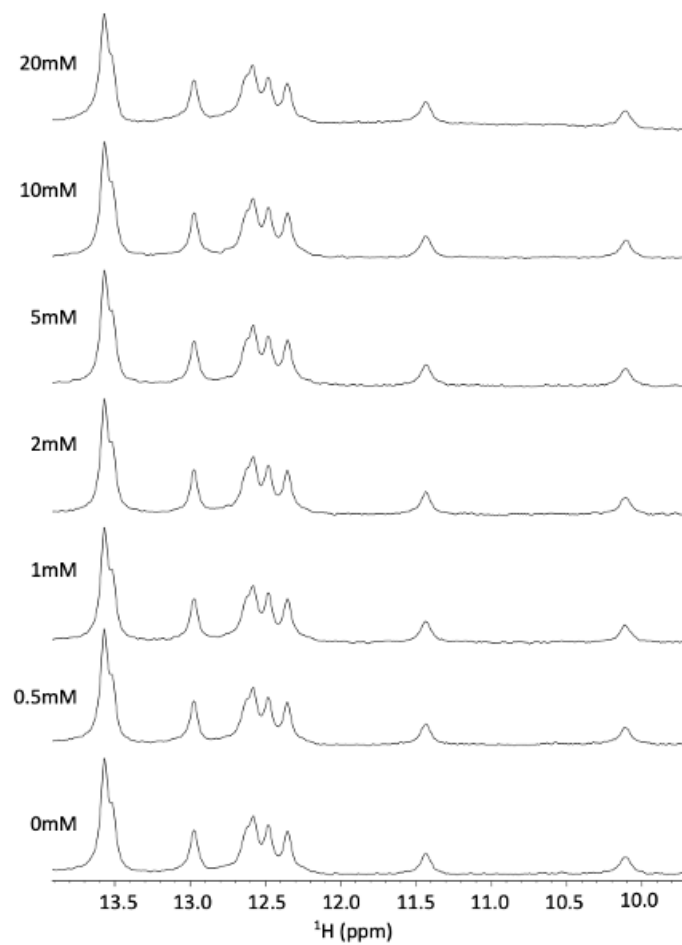


Figure 3.3.7 Titration of Glumod-6 with Glucose. With each addition of glucose, no new signals or chemical shift changes in imino peak region observed therefore no binding was observed. Glumod-6 500mM, buffer conditions: 250mM NaCl, 10mM  $\text{H}_2\text{Na}_2\text{PO}_4$ , pH 7.6, 10%  $\text{D}_2\text{O}$ .

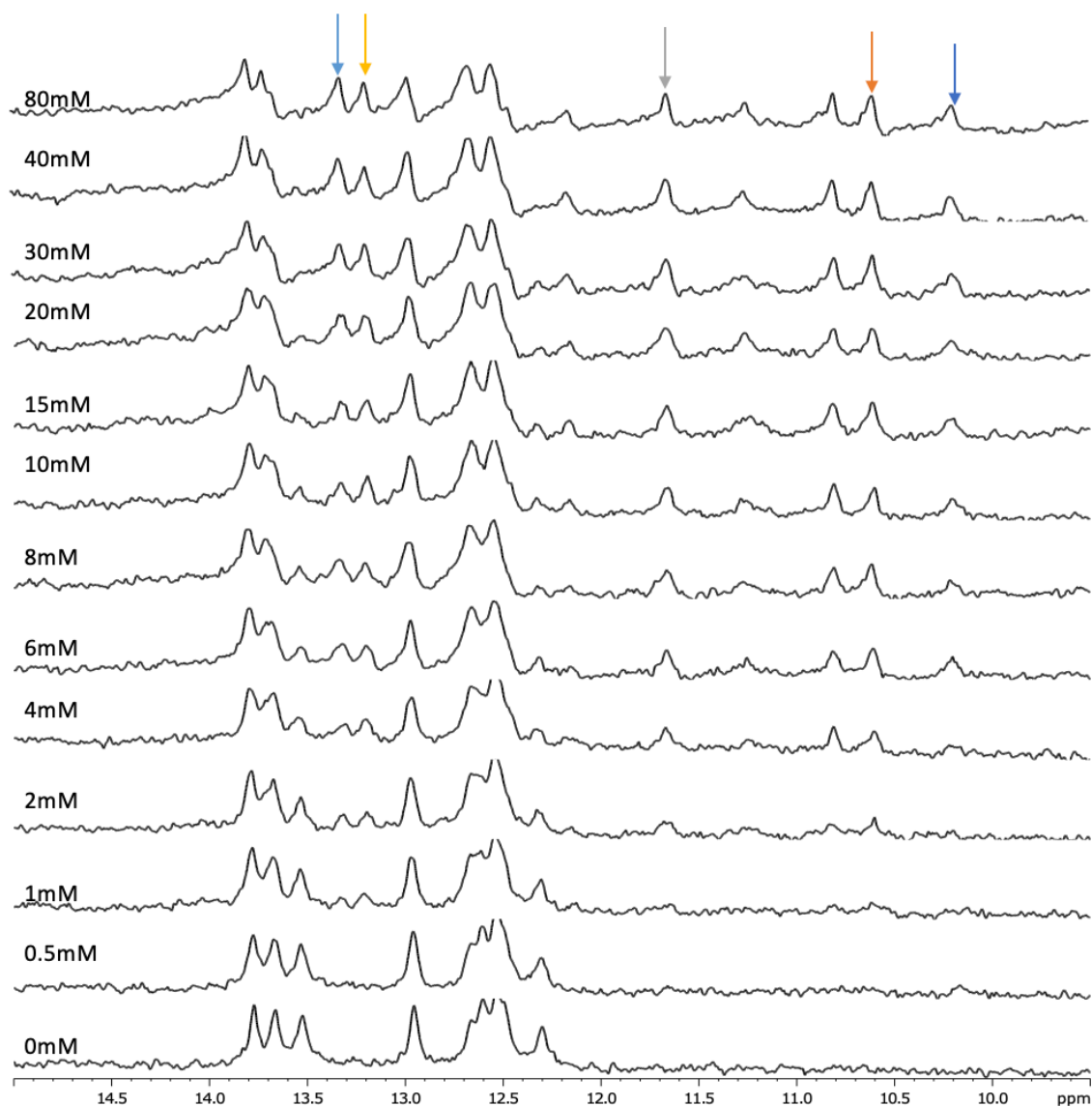


Figure 3.3.8 Titration of Glumod-7 with Glucose. With each addition of glucose, new imino peaks were observed thereby indicating binding. Glumod-7 500mM, buffer conditions: 250mM NaCl, 10mM  $\text{H}_2\text{N}_2\text{PO}_4$ , pH 7.6, 10%  $\text{D}_2\text{O}$ . The coloured arrows correspond to the new imino proton signals seen with the addition of glucose and to the data points in figure 3.3.9.

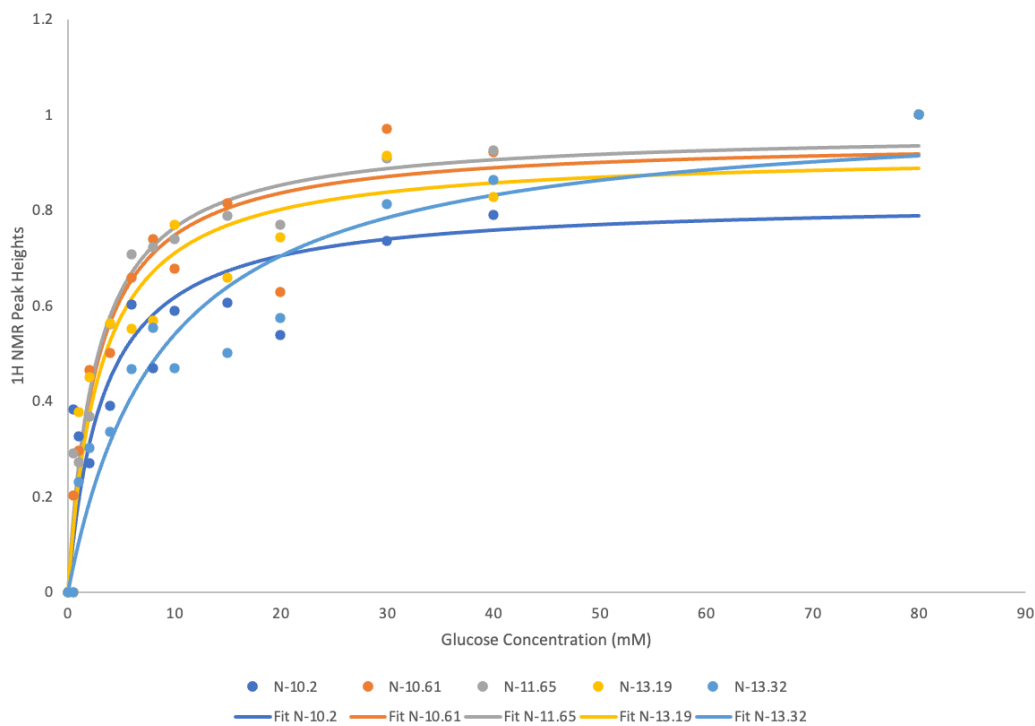


Figure 3.3.9 Titration curve of Glumod-7. Data acquired from NMR Spectra, analyzed using Sigmaplot fit to 1 site binding. The overlaid plots of the imino protons fit to the equation that describes 1:1 binding of glucose and Glumod-7 (see section 2.5).

Table 3.3.1 Glumod-7 Normalized Signal Statistics. Grubb's test done to exclude outlier 13.31 from average. Grubb value of 1.78, as the  $G_{\text{test}}$  was great than the  $G_{\text{critical}}$  (1.67) the data point was rejected as an outlier. The  $G_{\text{critical}}$  is for a 95% confidence interval with 5 samples.

Immino Proton Signal	R-square	$K_d$ (mM)
13.31	0.9	8.8
13.19	0.9	3.0
11.65	1	2.7
10.61	0.9	2.7
10.2	0.8	3.3
Average	0.9	2.9
Standard Deviation	0.07	0.3

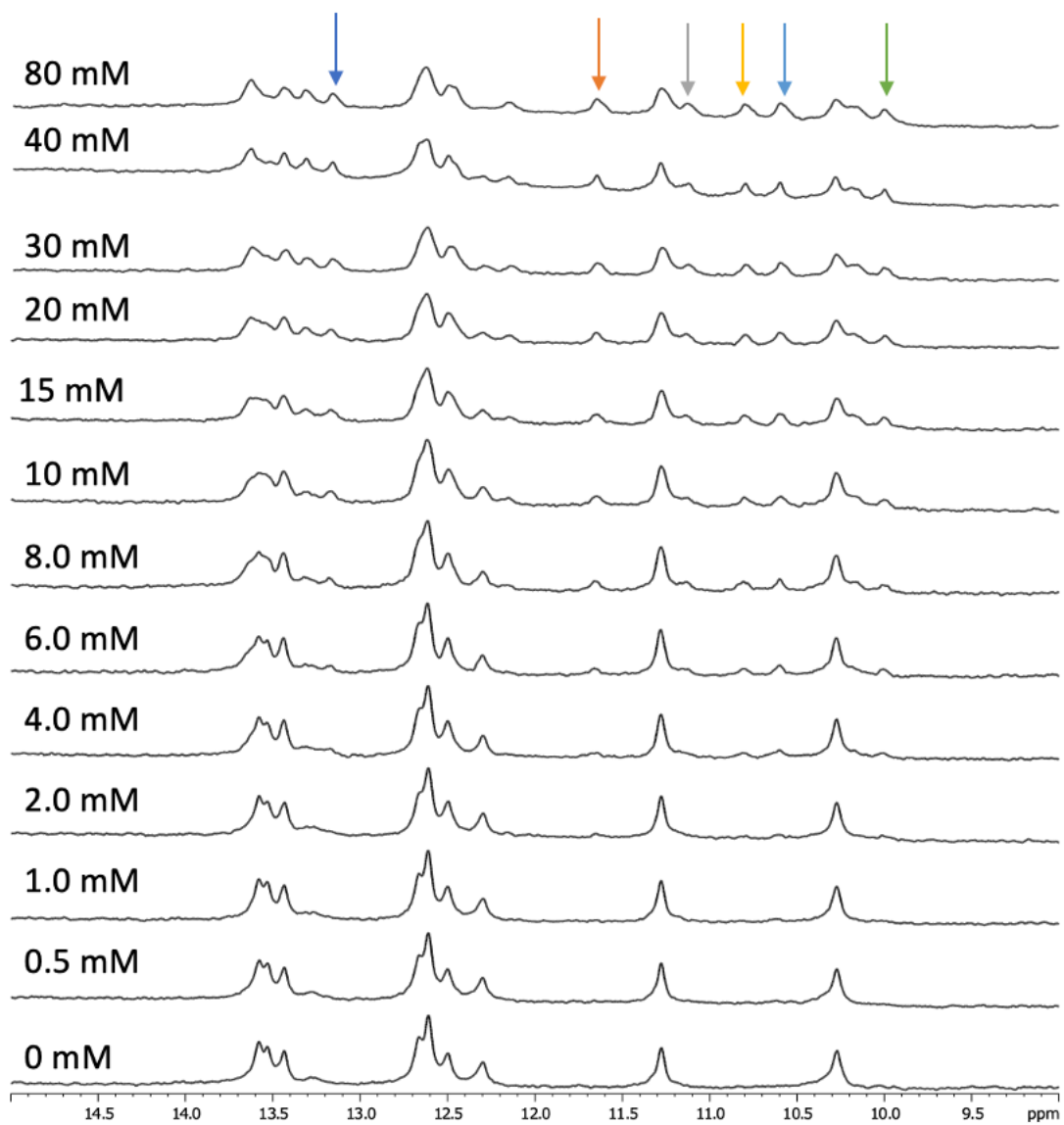


Figure 3.3.10 Titration of Glumod-8 with Glucose. With each addition of glucose, new imino peaks were observed thereby indicating binding. Glumod-8 500mM, buffer conditions: 250mM NaCl, 10mM H<sub>2</sub>Na<sub>2</sub>PO<sub>4</sub>, pH 7.6, 10% D<sub>2</sub>O. The coloured arrows correspond to the new imino proton signals seen with the addition of glucose and to the data points in figure 3.3.11.

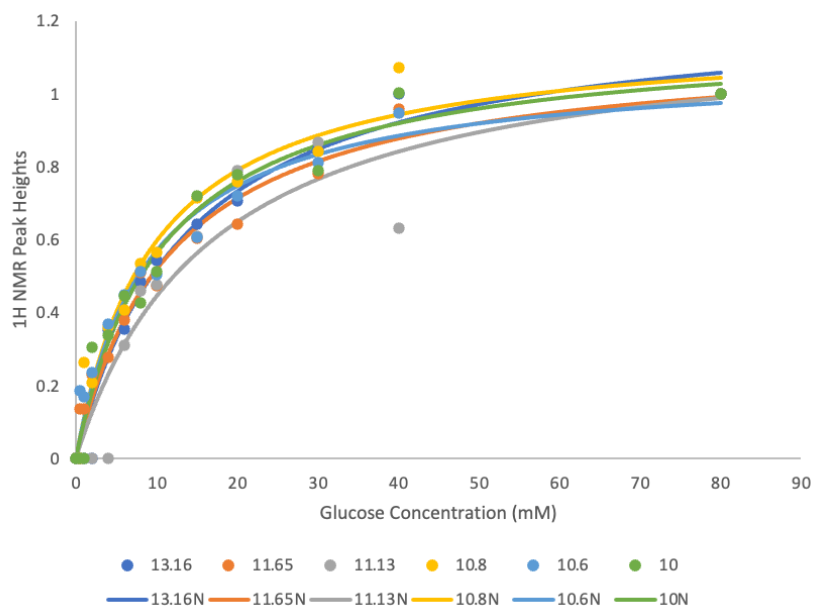


Figure 3.3.11 Titration curve of Glumod-8. Data acquired from NMR Spectra, analyzed using Sigmaplot fit to 1 site binding. The overlaid plots of the imino protons fit to the equation that describes 1:1 binding of glucose and Glumod-8 (see section 2.5).

Table 3.3.2: Glumod-8 Normalized Signal Statistics.

Immino Proton Signal	R-square	$K_d$ (mM)
13.16	0.97	14.0
11.65	0.97	12.0
11.13	0.90	17.0
10.8	0.97	9.6
10.6	0.97	9.1
10	0.97	10.7
Average	0.96	12.0
Standard Deviation	0.03	3.0

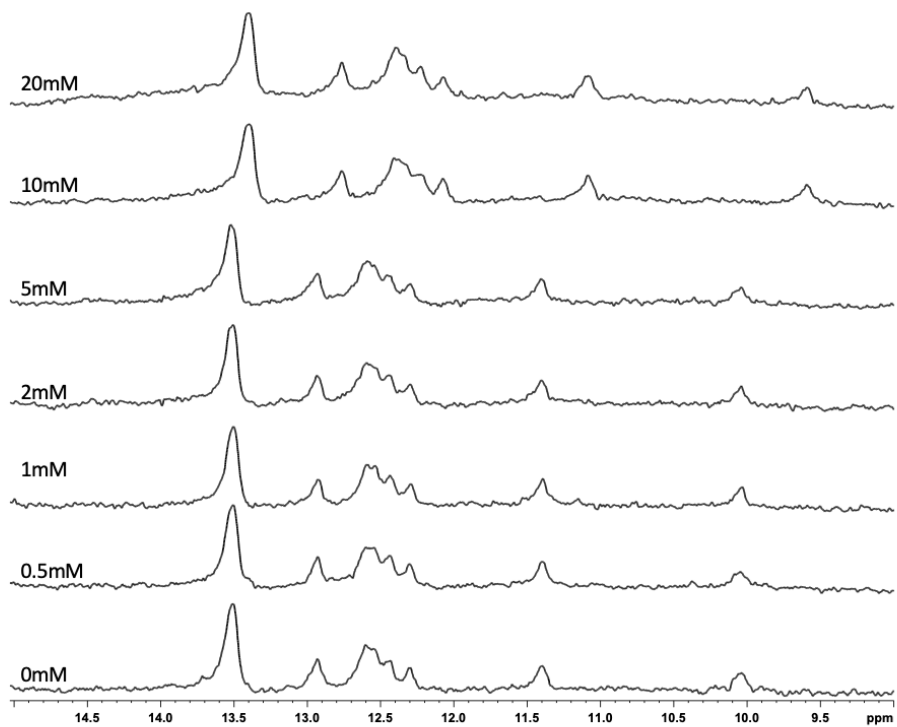


Figure 3.3.12 Titration of Glumod-9 with Glucose. With each addition of glucose, no change in imino peaks observed and no change in chemical shifts therefore no binding was observed. Glumod-9 500mM, buffer conditions: 250mM NaCl, 10mM  $H_2Na_2PO_4$ , pH 7.6, 10%  $D_2O$ .

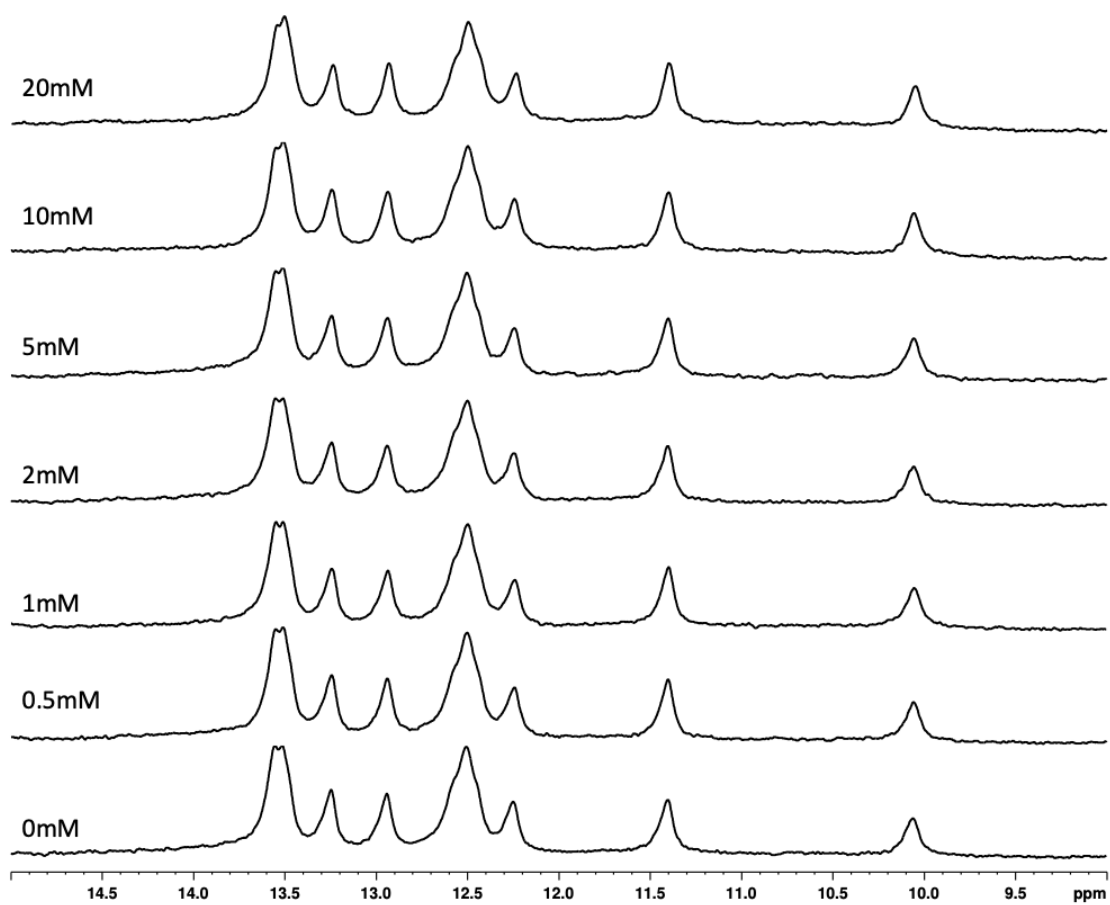


Figure 3.3.13 Titration of Glumod-10 with Glucose. With each addition of glucose, no change in imino peaks observed and no change in chemical shifts therefore no binding was observed. Glumod-10 500mM, buffer conditions: 250mM NaCl, 10mM  $H_2Na_2PO_4$ , pH 7.6, 10%  $D_2O$ .

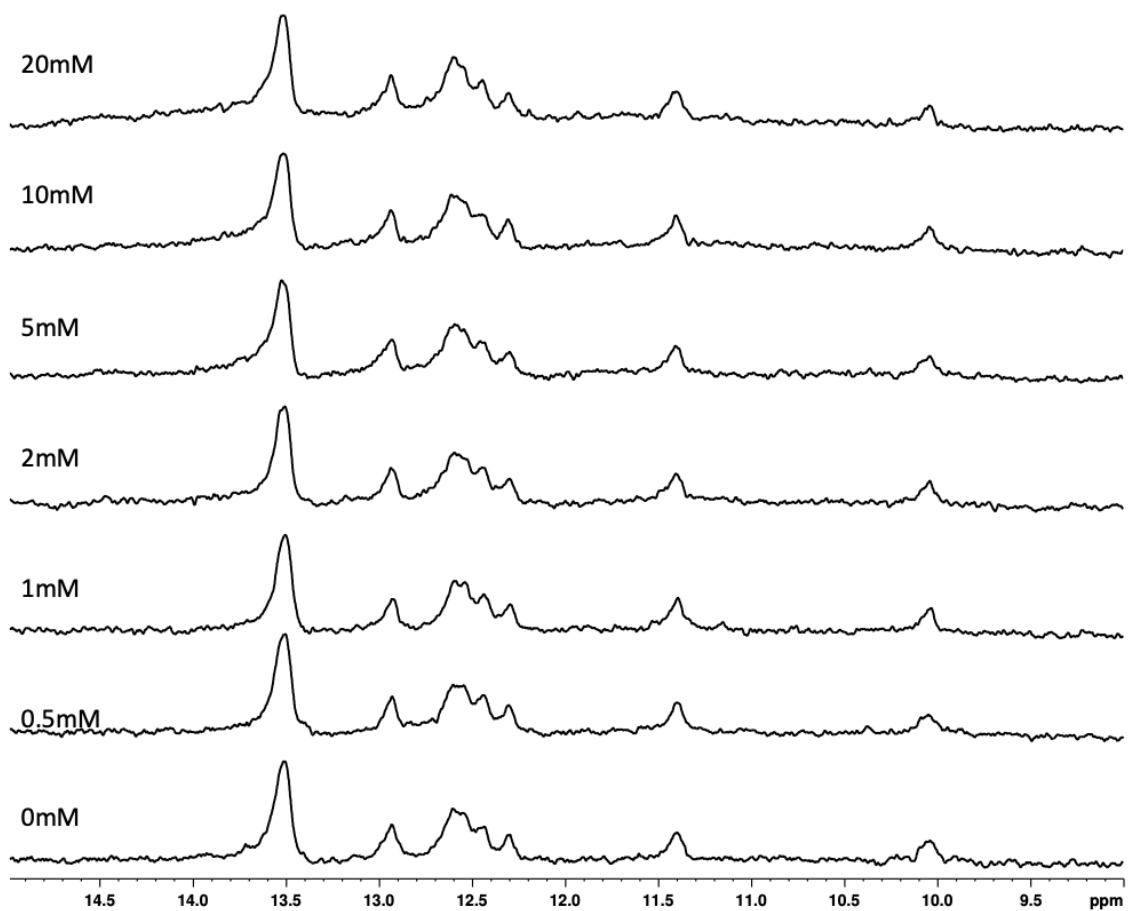


Figure 3.3.14 Titration of Glumod-11 with Glucose. With each addition of glucose, no change in imino peaks observed and no change in chemical shifts therefore no binding was observed. Glumod-11 500mM, buffer conditions: 250mM NaCl, 10mM  $\text{H}_2\text{N}_2\text{PO}_4$ , pH 7.6, 10%  $\text{D}_2\text{O}$ .

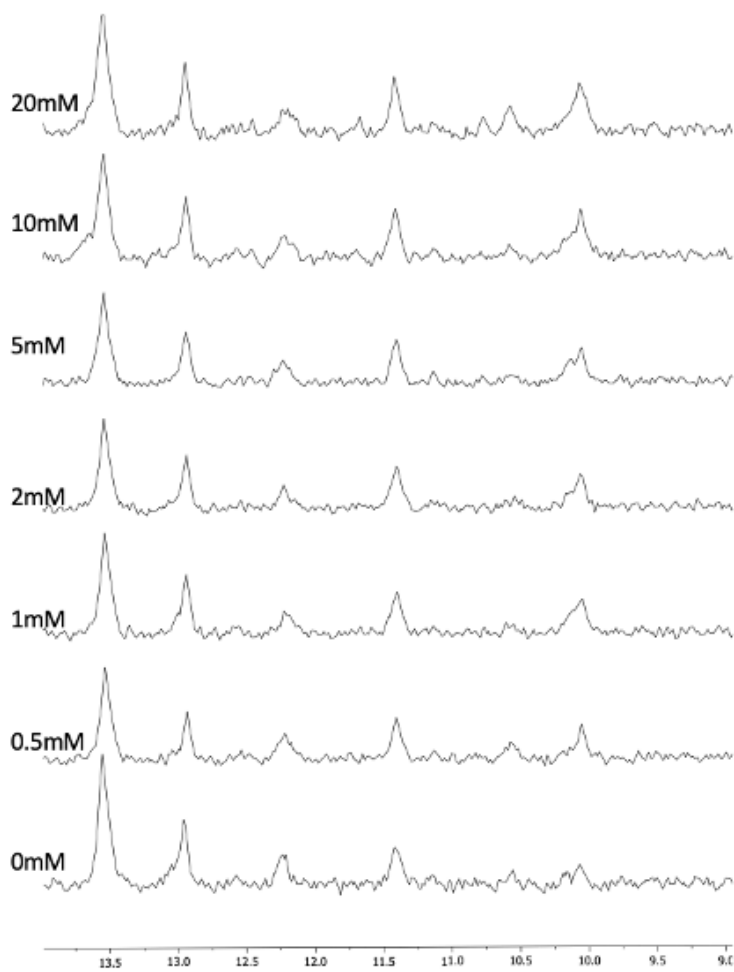


Figure 3.3.15 Titrations of Glumod-12 with Glucose. With each addition of glucose, a change in imino peaks was observed thereby indicating binding. Glumod-12 500mM, buffer conditions: 250mM NaCl, 10mM  $\text{H}_2\text{Na}_2\text{PO}_4$ , pH 7.6, 10%  $\text{D}_2\text{O}$ .

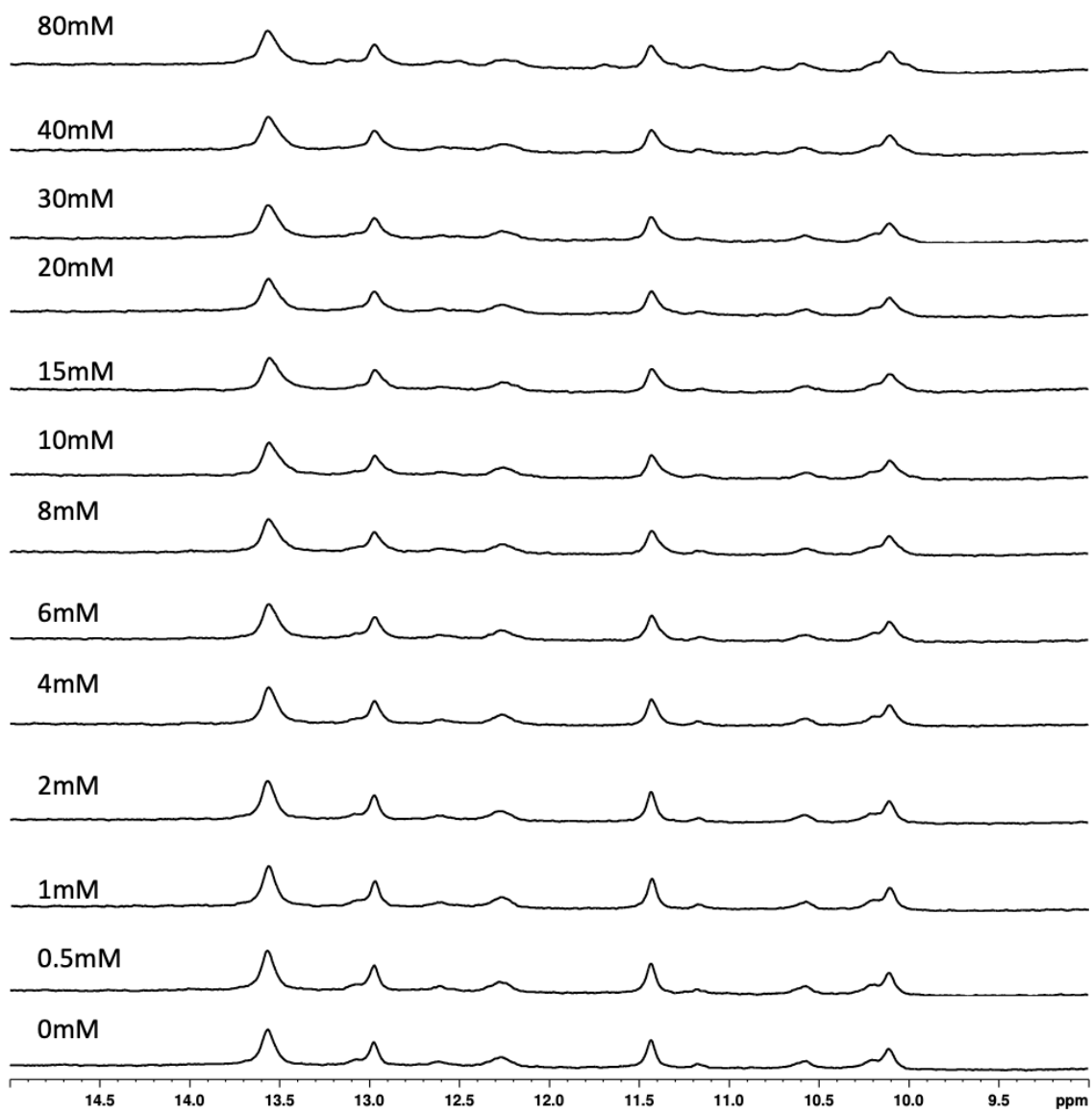


Figure 3.3.16 Further Titrations of Glumod-12 with Glucose.

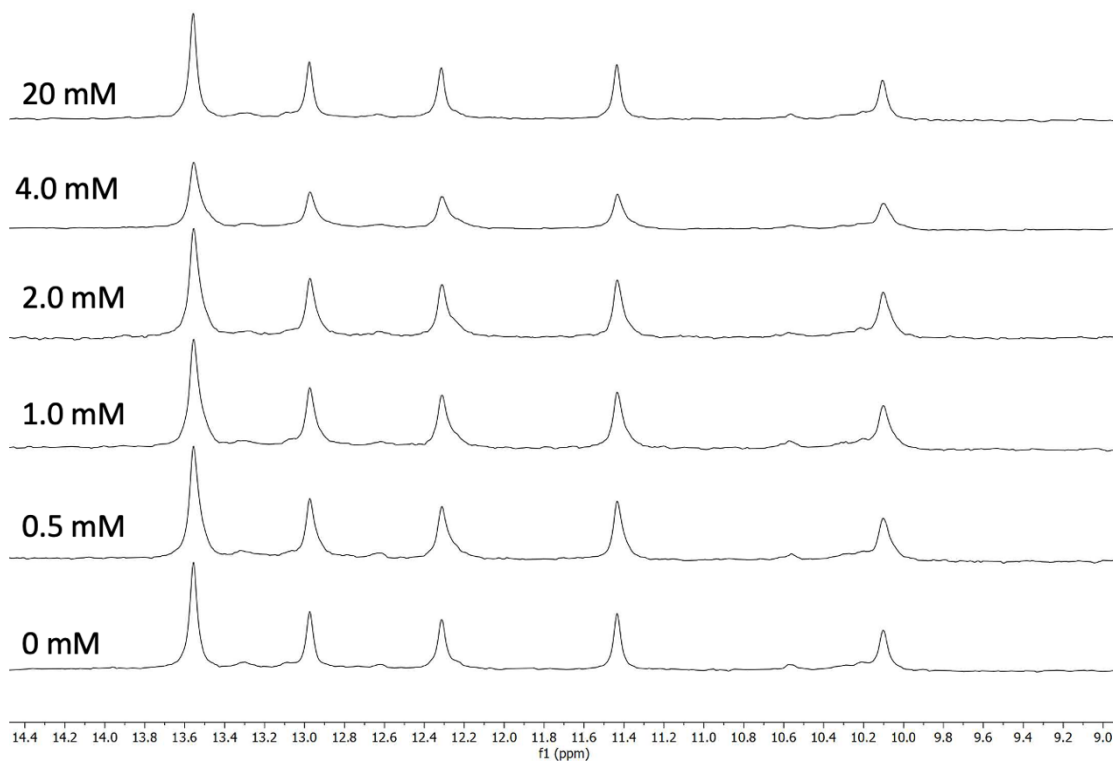


Figure 3.3.17 Titrations of Glumod-13 with Glucose. With each addition of glucose, no change in imino peaks was observed and no change in chemical shifts therefore no binding was observed. Glumod-11 500mM, buffer conditions: 250mM NaCl, 10mM  $\text{H}_2\text{N}_2\text{PO}_4$ , pH 7.6, 10%  $\text{D}_2\text{O}$ .

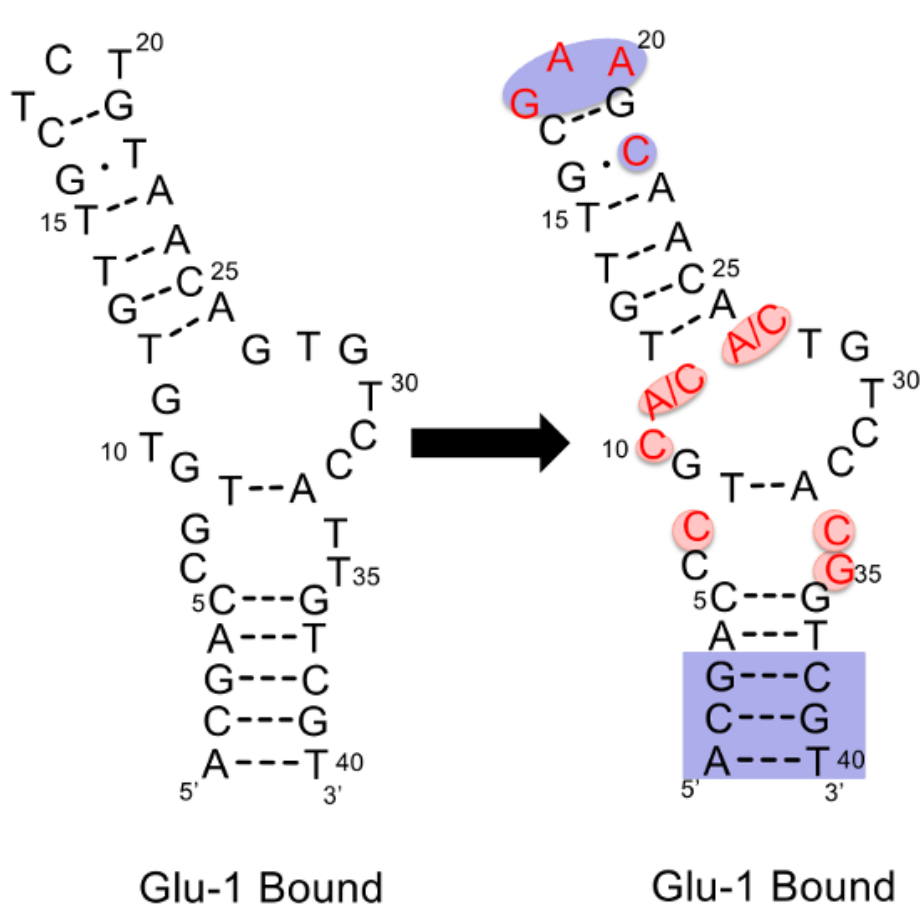


Figure 3.3.18 Secondary Structures of Free state Glucose-Binding Aptamer Modifications. The modifications were created in the Johnson Lab with the goal of identifying a substitution in a base that would cause the glucose binding aptamer to have a higher affinity for glucose. The wild type glucose-binding aptamer is denoted as Glu-1 with every subsequent modification highlighted in red. The modifications highlighted in red denoted no binding observed while those in blue denote binding observed. These results were obtained through titrations with glucose. Bases 1, 2, 3, 38, 39, and 40 were removed from the bottom helix and binding was still observed.

### 3.4 Concluding Remarks

Previously published studies have looked at a glucose-binding aptamer (Glu-1) in terms of binding affinity and stability. There remained a need to further modify this aptamer as it is stable from 5-30°C which solves the issue of long-term stability *in vivo* of current biosensors on the market. In this study, it was demonstrated that nucleic acid modifications were unable to significantly improve the binding affinity of Glu-1. There were only 3 binding sequences which bound glucose: Glumod-7, Glumod-8, and Glumod-12. While Glumod-12 bound, it had very weak

binding insufficient to further analyze the binding affinity of the modification. The binding affinity was lowered with Glumod-8 as the  $K_d$  increased from  $5\text{mM}\pm 2\text{mM}$  to  $12\text{mM}\pm 3\text{mM}$ . Therefore, it would not be beneficial to continue studying this sequence. The binding affinity was increased with Glumod-7 as the  $K_d$  decreased from  $5\text{mM}\pm 2\text{mM}$  to  $2.9\text{ mM}\pm 0.3\text{mM}$ . Unfortunately, this increase of binding affinity was not significantly different from the Glu-1 reported  $K_d$  and therefore would not be ideal to continue with this sequence unless further tested in terms of stability by NMR thermomelts. Furthermore, we demonstrated that the binding pocket of glucose is much larger than originally hypothesized to solely include the top of the center bulge region and most likely includes the whole bulge region (figure 1.9). This was concluded as modifications made to nucleic acids 10,11, and 27 at the top of the bulge destroyed binding, as well as modifications made to nucleic acids 7, 34, 35 at the bottom of the bulge region that also destroyed binding. It could be that not every nucleotide in the binding pocket interacts directly with the glucose molecule rather could be assisting with secondary interactions which aid in binding. Therefore, it can be concluded that the parent aptamer Glu-1 is currently optimized for binding glucose and is not susceptible to nucleic acid alterations within, close or far from the hypothesized binding site (figure 1.9). While the aptamer does originally bind within the body's blood glucose concentration at  $5^\circ\text{C}$ , the need to increase the affinity remains as the aptamer might perform differently at  $37^\circ\text{C}$ . Furthermore, we studied the aptamer at  $5^\circ\text{C}$  as we are interested in other situations in which it could perform other than blood.

## **Chapter 4. Thermodynamic Properties of Cocaine-Binding Aptamers**

### **4.1 Preface**

All the data presented in this chapter was acquired and analyzed by me however previous members in the lab have contributed to this research by conducting preliminary studies.

### **4.2 Introduction**

Aptamers are single stranded oligonucleotides which are selected to bind a particular target ligand which ranges from small molecules to cells. Aptamers are applicable in medical and analytical fields as they tend to bind with high affinity and selectivity to their targets.

The cocaine-binding aptamer series is composed of three stems extending from a three-way junction formed around two noncanonical A-G base pairs (figure 1.7). This series is unique as the structure switches from preformed in the free state to folding in the presence of the ligand dependent on the number of base pairs in stem one. With 3 or fewer base pairs present in stem one, there is a ligand-induced structure-switching mechanism such as in MN19 while with 4 or more base pairs present in stem one the structure is largely preformed such as in MN4<sup>32</sup>. The cocaine-binding series has a higher affinity to quinine and other quinine-based antimalarial compounds than cocaine itself<sup>37</sup>. The aptamers studied in this project were previously modified by the Johnson Lab at York University. These modifications include changes to stem 2 and stem 3, alterations to salt concentration, temperature, pH conditions, and buffer conditions. The purpose of this project is to identify if there is a correlation between the stem one length and stability of the cocaine-binding aptamer.

### 4.3 Results and Discussion

OR7 with one base pair in stem one (figure 1.8) did not show any analyzable signal in the free or the quinine bound state (supplementary, figure 2). It demonstrated signal similar to a buffer-buffer run (see supplementary, figure 1). Therefore, no results were obtained from these experiments at 90 $\mu$ M or 180 $\mu$ M.

OR8 with two base pairs in stem one (figure 1.8) showed an analyzable signal solely in the bound state (figure 4.3.1). This was predicted as previously published data showed that this aptamer has a structure-switching mechanism<sup>32</sup>. The bound signal was then analyzed to produce a thermogram (figure 4.3.1) to give insights into the thermodynamic properties of the aptamer. OR8 has a  $T_m$  of 67°C  $\pm$ 1°C which is the temperature at which the structure unfolds,  $\Delta H$  was -220kJ/mol  $\pm$ 12kJ/mol determined by fitting the signal to a sigmoidal curve and the area under the curve is the enthalpy. The previously reported  $T_m$  is 28°C  $\pm$ 1 which used the method of UV melts<sup>53</sup>. We are unsure why the melt temperature in the bound state is so high though this data is from 10 scans on different days with different samples and requires further investigation.

MN19 with three base pairs in stem one (figure 1.8) only showed a signal in the bound state as expected (figure 4.3.1). This result agrees with previously published data that concluded that the majority of the structure is formed with ligand binding<sup>32</sup>. MN19 has a  $T_m$  of 48.0°C  $\pm$ 0.2°C which is the temperature at which the structure unfolds,  $\Delta H$  was -247.0kJ/mol  $\pm$ 0.1kJ/mol (table 4.3.1). The melt temperature indicates it unfolds at a lower temperature than OR8 though with a higher  $\Delta H$  is indicating a greater stability shift between the free and bound state. The trends of these results agree with previously published data though the numerical values differ. These results vary from previously published data where  $\Delta H$  was reported to be -23.9 $\pm$ 0.9 kcal/mol<sup>32</sup> and 26 $\pm$ 0.3

kcal/mol<sup>54</sup>. As the DSC reported value is -58.9 kcal/mol which is an average of 5 scans and 2 concentrations (90 $\mu$ M and 180 $\mu$ M). In terms of melt temperature, I reported through DSC experiments for the melt temperature to be 48 $^{\circ}$ C $\pm$ 0.2 $^{\circ}$ C while previously published data using UV-vis reported a melt temperature of 35.5 $^{\circ}$ C $\pm$ 0.3 $^{\circ}$ C<sup>39</sup>.

OR9 with four base pairs in stem one (figure 1.8) showed signal both in the quinine bound state and the free state. This result agrees with previously published data indicating that this number of base pairs begins to have a preformed structure with small changes to the structure with ligand binding<sup>32</sup>. The bound and free signals were then analyzed to produce a thermogram (figure 4.3.1) to give insights into the thermodynamic properties of the aptamer. OR9 has a  $T_m$  of 56 $^{\circ}$ C  $\pm$ 0.6 $^{\circ}$ C in the bound state and a  $\Delta H$  was -291kJ/mol  $\pm$ 6kJ/mol (-69.6kcal/mol) (table 4.3.1). Previously reported data using UV melts, report a  $T_m$  of 44.1 $^{\circ}$ C  $\pm$ 0.4 and a enthalpy of -7.3 $\pm$ 0.3 kcal/mol<sup>53</sup> which are significantly lower than our values. These values indicate that OR9 is more stable than MN19 which is one base pair less indicating that with the lengthening of stem one the stability increases similar to the previously published binding affinity trend<sup>32</sup>.

OR10 with five base pairs in stem one (figure 1.8) showed signal both in the quinine bound state and the free state (figure 4.3.1). This result agrees with previously published data indicating that this number of base pairs begins to have a preformed structure with small changes to the structure with ligand binding<sup>32</sup>. OR10 has a  $T_m$  of 62 C  $\pm$ 0.1 $^{\circ}$ C in the bound state and a  $\Delta H$  was -343kJ/mol  $\pm$ 10kJ/mol (-82kcal/mol) (table 4.3.1). Previously published data reported a  $T_m$  of 53.1 $^{\circ}$ C  $\pm$ 0.4 and an enthalpy of -6.3 $\pm$ 0.2 kcal/mol which is significantly lower than our values. These values indicate that the stability is increasing with each addition of base pairs to stem one length.

MN4 with six base pairs in stem one (figure 1.8) showed signal in both the quinine bound and free state (figure 4.3.1). This result agrees with previously published data indicating that this number of base pairs begins to have a preformed structure with small changes to structure with ligand binding<sup>32</sup>. MN4 has a  $T_m$  of  $63^\circ\text{C} \pm 0.05^\circ\text{C}$  in the bound state and a  $\Delta H$  was  $-495\text{kJ/mol} \pm 8\text{kJ/mol}$  (table 4.3.1). The thermogram produced by these experiments can be seen in figure 4.3.1. The melt temperature agrees with previously published data which reported a  $T_m$  of  $61^\circ\text{C}$  using UV-vis methods<sup>32</sup>. The enthalpy does not agree with previously published results as  $-59\text{kcal/mol}$  is significantly greater than the reported  $-14 \pm 0.2\text{kcal/mol}$ .

OR11 with seven base pairs in stem one (figure 1.8) showed signal in both the quinine bound and free state. The results disagreed with previously published hypothesized data indicating that this number of base pairs would be more stable than MN4<sup>32</sup> as it has one additional base pair. OR11 has a  $T_m$  of  $66^\circ\text{C} \pm 0.2^\circ\text{C}$  in the bound state and a  $\Delta H$  was  $-359\text{kJ/mol} \pm 11\text{kJ/mol}$  ( $85.8\text{kcal/mol}$ ). The thermogram produced by these experiments can be seen in figure 4.3.1. The previously reported  $T_m$  is  $62.1^\circ\text{C} \pm 0.2$  and an enthalpy of  $-4.9 \pm 0.2\text{kcal/mol}$ <sup>53</sup>. While the enthalpy is significantly different though reported at  $10^\circ\text{C}$  compared to  $20^\circ\text{C}$  the melt temperatures are relatively close. This dip in stability requires further investigation which could be done using UV-vis melts at the same conditions to validate the results.

The calculated dissociation constant from DSC experiments were not in agreement with previous studies on these aptamers<sup>32,54</sup>. DSC  $K_d$  values were significantly lower for reference to  $\#^{-23}\mu\text{M}$  which is very tight binding though most likely incorrect. This led us to hypothesize why this was happening even with the preformed structured aptamers this result was seen. Our hypothesis coming from these results is that there is another component to the preformed structure

which results in conformational changes thereby affecting the  $K_d$ . Though this hypothesis requires further experiments for validation which would include NMR and ITC studies

Previous experiments in the Johnson lab on the cocaine-binding aptamers show differences in affinity ( $K_d$ ) based on the stem one length<sup>32</sup>. This was done using a method called isothermal titration calorimetry (ITC). The hypothesized trend was that as the length of stem one was increased from 1 to 7 base pairs the stability would increase as well<sup>33</sup>. The question which remained was how the stem lengths overall affected the stability of the molecules. They hypothesized a staircase-like trend of Gibbs free energy from OR7 (1bp) to OR11 (7bp)<sup>55</sup>. Through DSC thermodynamics we were able to assign values to this staircase and demonstrate a new trend. This trend would be the initial increasing of stability until 6 base pairs then the decreasing of stability after six base pairs in stem one of cocaine-binding aptamers (figure 4.3.2).

MN4 had the largest difference between  $\Delta G$  values therefore leading to a larger than expected  $K_d$ . The  $K_d$  reported from ITC experiments<sup>39</sup> (table 4.3.1) is much larger than the  $K_d$  calculated from the  $\Delta\Delta G$  of DSC experiments. This could be due to a lack of structure in the free state though requires further investigation. The difference in  $\Delta G$  hypothesized would be similar between the preformed structures of cocaine-binding aptamers. Though through figure 4.3.2 it was seen that each preformed aptamer had a significant difference in  $\Delta\Delta G$ . A trend was seen as the  $\Delta\Delta G$  value increased through the addition of base pairs from OR9 to MN4 before decreasing again in OR11 which corresponds to previously published binding affinity ITC data seen in table 4.3.1.

Through the DSC thermodynamic experiments unusual results were seen. Our values were significantly higher than previously reported values at 10°C using UV melts. This could be due to the differences in experimental methods or temperatures reported at. Though the values reported in this thesis were performed as an average of 5 scans, repeated in duplicates on different days

with different samples. Another result which was unexpected was the decrease of stability seen at 7 base pairs as we believed the aptamer would become more stable with each addition. This loss of stability could be due to three-dimensional structure folding interactions which destabilize the molecule therefore more free energy would be required for stability that decreases the  $K_d$ . This trend was also seen in the decrease of affinity with 7 base pairs. Therefore, further investigation is required for explanation on why this phenomenon is observed.

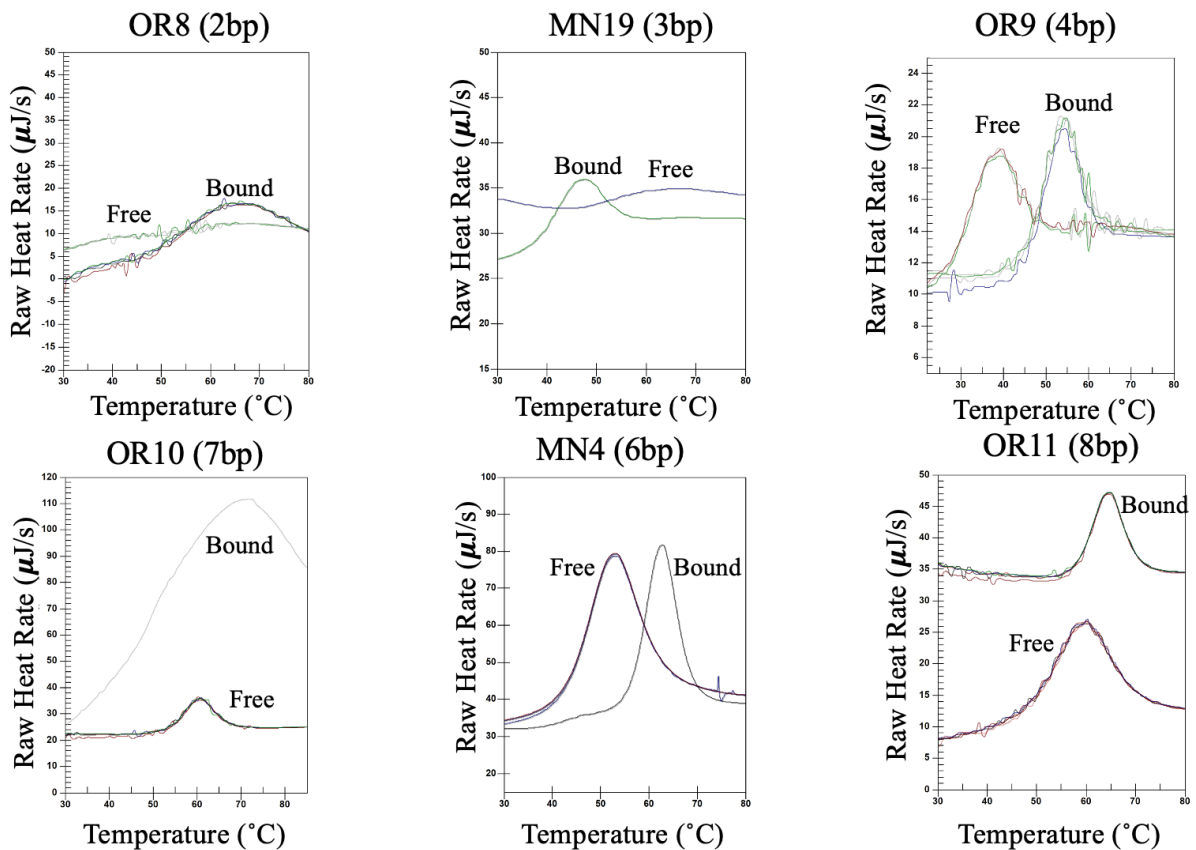


Figure 4.3.1 Analysed Thermograms of Stem One cocaine-binding variants. OR8 demonstrates an unanalysable signal in the free state while an analysable signal is seen bound to 2.2mM quinine. MN19 does not show an analysable signal in the free state though an analysable thermogram is seen in the bound state to 2.2mM quinine. OR9 demonstrates an analysable thermogram in the free and bound states with the bound state melting at a higher temperature than the free state. OR10 demonstrates an analysable thermogram in the free and bound state with the bound state showing a greater enthalpy and melt temperature than the free state. MN4 demonstrates an analysable thermogram in the free and bound state with the bound state having a higher melt temperature though a similar enthalpy to the free state. OR11 has an analysable thermogram in the free and bound state demonstrating a higher melt temperature in the bound state though the free state shows a higher enthalpy.

Table 4.3.1 Stability Analysis of cocaine-binding stem one variant aptamers. Represented is the data obtained through duplicates of DSC 10 scan experiments with the average of the included scans shown. The melt temperature,  $\Delta H$  and  $C_p$  are obtained from the analysis software while the  $\Delta S$ ,  $\Delta G$ , and the  $K_d$  were calculated values. This data is obtained in the bound state with 0.18mM aptamer bound to 2.2mM Quinine. Differences in  $K_d$  were seen in the data obtained from the DSC vs. the ITC indicate there is more to consider than ligand binding.

Aptamer	OR7	OR8	MN19	OR9	OR10	MN4	OR11
$\Delta H$ (kJ/mol)	vwb	-220 $\pm$ 12	-246.6 $\pm$ 0.1	-290 $\pm$ 6	-344 $\pm$ 10	-495 $\pm$ 8	-359 $\pm$ 11
$\Delta S$ (kJ/mol/ $^{\circ}$ K)	vwb	-3.2 $\pm$ 0.2	-5.1 $\pm$ 0.1	-5.20 $\pm$ 0.2	-5.6 $\pm$ 0.2	-7.9 $\pm$ 0.1	-5.0 $\pm$ 0.2
$\Delta G$ (kJ/mol) At 10 $^{\circ}$ C	vwb	-122 $\pm$ 7	-92 $\pm$ 2	-134 $\pm$ 1	-176 $\pm$ 5	-258 $\pm$ 5	-195 $\pm$ 6
$\Delta C_p$ (kJ/mol/ $^{\circ}$ K)	vwb	-0.3 $\pm$ 0.3	-1.3 $\times 10^1$ $\pm$ 0.8	-2 $\pm$ 1	-8.2 $\pm$ 1	-36 $\pm$ 4	-14 $\pm$ 1
Melt Temp ( $^{\circ}$ C)	vwb	67 $\pm$ 1	48.0 $\pm$ 0.2	55.8 $\pm$ 0.6	61.7 $\pm$ 0.1	62.6 $\pm$ 0.1	65.8 $\pm$ 0.2
$K_d$ ( $\mu$ M) ITC	vwb	11.2 $\pm$ 0.5	0.23 $\pm$ 0.09	0.21 $\pm$ 0.06	0.13 $\pm$ 0.04	0.15 $\pm$ 0.06	0.14 $\pm$ 0.07

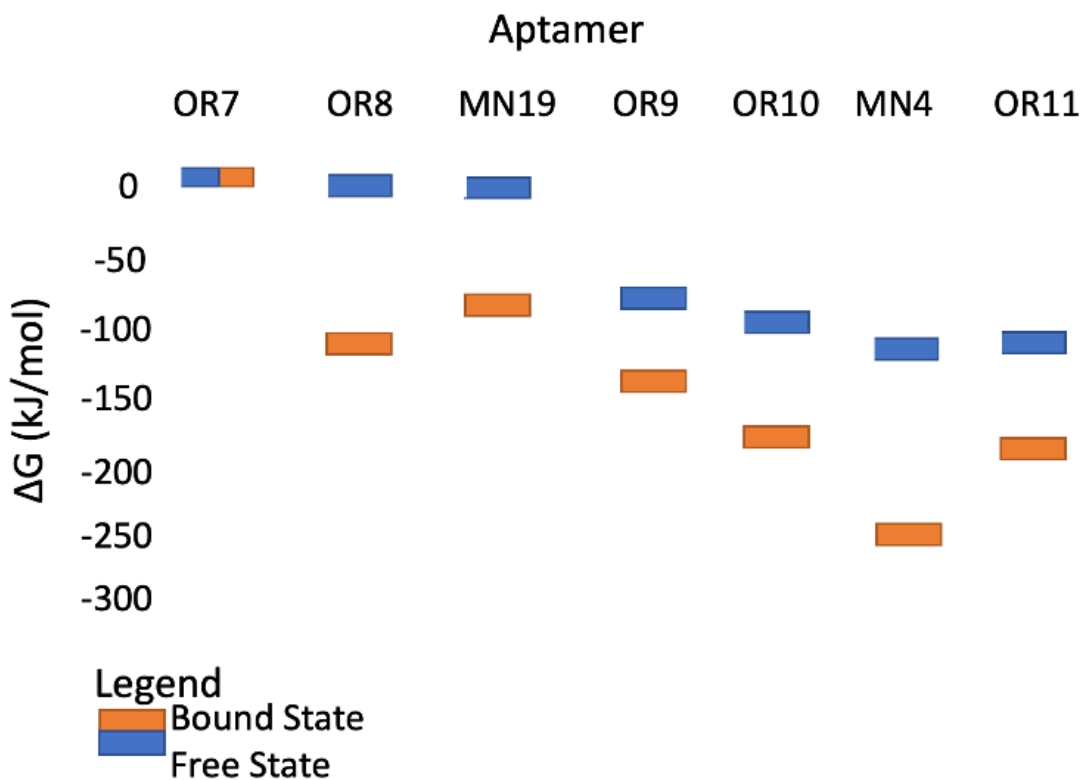


Figure 4.3.2  $\Delta G$  unfolding of stem one variants of cocaine-binding aptamers. Through DSC experiments the  $\Delta G$  of the stem one variants were calculated. Demonstrated here is the staircase trend though broken by MN4. Determined through multiple analysis that MN4 is the most thermodynamically stable stem one variant with the least stable being OR7 with its very weak binding (VWB).

#### 4.4 Concluding Remarks

OR7 did not demonstrate analysable data in the free or the quinine-bound state (supplemental, figure 2). The free vs. the quinine bound states of the aptamers are compared to determine an aptamer's overall stability. Stability refers to all studied thermodynamic parameters:  $\Delta H$ ,  $\Delta S$ ,  $\Delta G$ ,  $T_m$ ,  $C_p$ . The experiments with OR8 indicate that it was the least stable molecule in the stem one variant group of those that had observable signals, with very weak binding observed in the free state and unusual values for the thermodynamic parameters seen in Table 4.3.1. Each addition of a base pair onto stem one increased the stability of the aptamer both in the free and quinine-bound states though decreased following the addition of six base pairs. The free states of

the stem one variants were determined to be less stable than those of the bound states. Furthermore, there seems to be more to consider than ligand-aptamer interactions for the binding affinity as significant differences were seen in values obtained from ITC and those calculated from difference in  $\Delta G$  with the DSC where further investigation is required using NMR, ITC, and UV-vis methods to further characterize the structure in the free and bound state.

This study demonstrated the differences seen in stability seen between the structure-switching aptamers (with less than 3 base pairs) and the preformed aptamers (those with 4 or greater base pairs). In agreement with previous studies done by the Johnson Lab<sup>32</sup>, we found that MN4 is the most stable cocaine-binding aptamer.

## Chapter 5. Future Work

In the glucose-binding aptamer project, we determined that the parent aptamer Glu-1 is not susceptible to sequence changes to improve its affinity. As only three nucleic acid modifications bound to glucose though two showed a decrease in binding affinity therefore stability of these sequences was not studied. As Glumod-7 demonstrated close binding affinity to the parent aptamer Glu-1, the next step would be to study the stability using NMR thermomelts. With the weak binding affinity NMR is the most suitable technique. Further steps would be to continue studying the Glu-1 and the Glumod-7 sequences as E-AB sensors to determine if the aptamer would be able to perform successfully *in vivo* conditions. Any tighter binding Glumod would additionally need to be tested to ensure that the specificity of the aptamer was retained.

In the cocaine-binding aptamer project, we established the trend of the increase of stability with the increase of base pairs in stem one. Further studies would also need to evaluate the decrease in stability seen after the addition of six base pairs to stem one. These experiments would need to look further at the structure and binding affinity of six plus base pairs to further understand this phenomenon.

## Bibliography

1. Cerchia, L., Giangrande, P. H., McNamara, J. O. & de Franciscis, V. Cell-Specific Aptamers for Targeted Therapies. *Methods Mol. Biol. Clifton NJ* **535**, 59–78 (2009).
2. Janas, T. & Janas, T. The selection of aptamers specific for membrane molecular targets. *Cell. Mol. Biol. Lett.* **16**, 25–39 (2010).
3. Yakovchuk, P., Protozanova, E. & Frank-Kamenetskii, M. D. Base-stacking and base-pairing contributions into thermal stability of the DNA double helix. *Nucleic Acids Res.* **34**, 564–574 (2006).
4. White, R. R., Sullenger, B. A. & Rusconi, C. P. Developing aptamers into therapeutics. *J. Clin. Invest.* **106**, 929–934 (2000).
5. Mogensen, J. E., Wimmer, R., Larsen, J. N., Spangfort, M. D. & Otzen, D. E. The Major Birch Allergen, Bet v 1, Shows Affinity for a Broad Spectrum of Physiological Ligands \*. *J. Biol. Chem.* **277**, 23684–23692 (2002).
6. Shaw, J.-P., Kent, K., Bird, J., Fishback, J. & Froehler, B. Modified deoxyoligonucleotides stable to exonuclease degradation in serum. *Nucleic Acids Res.* **19**, 747–750 (1991).
7. Zheng, Y. & Sheppard, T. L. Half-Life and DNA Strand Scission Products of 2-Deoxyribonolactone Oxidative DNA Damage Lesions. *Chem. Res. Toxicol.* **17**, 197–207 (2004).
8. Gruenke, P. R., Alam, K. K., Singh, K. & Burke, D. H. 2'-fluoro-modified pyrimidines enhance affinity of RNA oligonucleotides to HIV-1 reverse transcriptase. *RNA* **26**, 1667–1679 (2020).
9. Corey, D. R. Chemical modification: the key to clinical application of RNA interference? *J. Clin. Invest.* **117**, 3615–3622 (2007).

10. Zhu, Q., Liu, G. & Kai, M. DNA Aptamers in the Diagnosis and Treatment of Human Diseases. *Molecules* **20**, 20979–20997 (2015).
11. Tucker, B. J. & Breaker, R. R. Riboswitches as versatile gene control elements. *Curr. Opin. Struct. Biol.* **15**, 342–348 (2005).
12. Tuerk, C. & Gold, L. Systematic Evolution of Ligands by Exponential Enrichment: RNA Ligands to Bacteriophage T4 DNA Polymerase. *Science* **249**, 505–510 (1990).
13. Ellington, A. D. & Szostak, J. W. In vitro selection of RNA molecules that bind specific ligands. *Nature* **346**, 818–822 (1990).
14. Riley, T. R. *et al.* SELEX-seq, a method for characterizing the complete repertoire of binding site preferences for transcription factor complexes. *Methods Mol. Biol. Clifton NJ* **1196**, 255–278 (2014).
15. Mayer, G. The Chemical Biology of Aptamers. *Angew. Chem. Int. Ed.* **48**, 2672–2689 (2009).
16. Eaton, B. E., Gold, L. & Zichi, D. A. Let's get specific: the relationship between specificity and affinity. *Chem. Biol.* **2**, 633–638 (1995).
17. Privalov, P. Thermodynamic problems in structural molecular biology. *Pure Appl Chem* **79**, 1445–1462 (2007).
18. Garvie, C. W. & Wolberger, C. Recognition of Specific DNA Sequences. *Mol. Cell* **8**, 937–946 (2001).
19. Trujillo, C. A., Nery, A. A., Alves, J. M., Martins, A. H. & Ulrich, H. Development of the anti-VEGF aptamer to a therapeutic agent for clinical ophthalmology. *Clin. Ophthalmol. Auckl. NZ* **1**, 393–402 (2007).

20. Bunka, D. H., Platonova, O. & Stockley, P. G. Development of aptamer therapeutics. *Curr. Opin. Pharmacol.* **10**, 557–562 (2010).
21. Ng, E. W. M. *et al.* Pegaptanib, a targeted anti-VEGF aptamer for ocular vascular disease. *Nat. Rev. Drug Discov.* **5**, 123–132 (2006).
22. Köhler, G. & Milstein, C. Continuous cultures of fused cells secreting antibody of predefined specificity. *Nature* **256**, 495–497 (1975).
23. Ansar, W. & Ghosh, S. Monoclonal Antibodies: A Tool in Clinical Research. *Indian J. Clin. Med.* **4**, IJCM.S11968 (2013).
24. Mallikaratchy, P., Stahelin, R. V., Cao, Z., Cho, W. & Tan, W. Selection of DNA ligands for protein kinase C- $\delta$ . *Chem. Commun.* 3229–3231 (2006) doi:10.1039/B604778E.
25. Xiao, Y., Lubin, A. A., Heeger, A. J. & Plaxco, K. W. Label-Free Electronic Detection of Thrombin in Blood Serum by Using an Aptamer-Based Sensor. *Angew. Chem.* **117**, 5592–5595 (2005).
26. Bock, L. C., Griffin, L. C., Latham, J. A., Vermaas, E. H. & Toole, J. J. Selection of single-stranded DNA molecules that bind and inhibit human thrombin. *Nature* **355**, 564–566 (1992).
27. Dauphin-Ducharme, P. *et al.* Redox Reporter - Ligand Competition to Support Signaling in the Cocaine-Binding Electrochemical Aptamer-Based Biosensor. *Chem. – Eur. J.* **29**, e202300618 (2023).
28. Rajendran, M. & Ellington, A. D. In vitro selection of molecular beacons. *Nucleic Acids Res.* **31**, 5700–5713 (2003).
29. Stojanovic, M. N., de Prada, P. & Landry, D. W. Aptamer-Based Folding Fluorescent Sensor for Cocaine. *J. Am. Chem. Soc.* **123**, 4928–4931 (2001).

30. Stojanovic, M. N. & Landry, D. W. Aptamer-Based Colorimetric Probe for Cocaine. *J. Am. Chem. Soc.* **124**, 9678–9679 (2002).
31. Celikbas, E., Balaban, S., Evran, S., Coskunol, H. & Timur, S. A Bottom-Up Approach for Developing Aptasensors for Abused Drugs: Biosensors in Forensics. *Biosensors* **9**, 118 (2019).
32. Neves, M. A. D., Reinstein, O. & Johnson, P. E. Defining a Stem Length-Dependent Binding Mechanism for the Cocaine-Binding Aptamer. A Combined NMR and Calorimetry Study. *Biochemistry* **49**, 8478–8487 (2010).
33. Neves, M., Reinstein, O., Saad, M. & Johnson, P. Defining the secondary structural requirements of a cocaine-binding aptamer by a thermodynamic and mutation study. *Biophys. Chem.* **153**, 9–16 (2010).
34. Van Riesen, A. J. *et al.* Visible Fluorescent Light-up Probe for DNA Three-Way Junctions Provides Host–Guest Biosensing Applications. *ACS Appl. Bio Mater.* **4**, 6732–6741 (2021).
35. Stojanović, M. N., Green, E. G., Semova, S., Nikić, D. B. & Landry, D. W. Cross-Reactive Arrays Based on Three-Way Junctions. *J. Am. Chem. Soc.* **125**, 6085–6089 (2003).
36. Reinstein, O. *et al.* Engineering a Structure Switching Mechanism into a Steroid-Binding Aptamer and Hydrodynamic Analysis of the Ligand Binding Mechanism. *Biochemistry* **50**, 9368–9376 (2011).
37. Slavkovic, S., Altunisik, M., Reinstein, O. & Johnson, P. E. Structure–affinity relationship of the cocaine-binding aptamer with quinine derivatives. *Bioorg. Med. Chem.* **23**, 2593–2597 (2015).

38. Slavkovic, S., Churcher, Z. R. & Johnson, P. E. Nanomolar binding affinity of quinine-based antimalarial compounds by the cocaine-binding aptamer. *Bioorg. Med. Chem.* **26**, 5427–5434 (2018).
39. Shoara, A. A. *et al.* Development of a thermal-stable structure-switching cocaine-binding aptamer. *Biochimie* **145**, 137–144 (2018).
40. Churcher, Z. R., Garaev, D., Hunter, H. N. & Johnson, P. E. Reduction in Dynamics of Base pair Opening upon Ligand Binding by the Cocaine-Binding Aptamer. *Biophys. J.* **119**, 1147–1156 (2020).
41. W. Harkness, R., Slavkovic, S., E. Johnson, P. & K. Mittermaier, A. Rapid characterization of folding and binding interactions with thermolabile ligands by DSC. *Chem. Commun.* **52**, 13471–13474 (2016).
42. Nakatsuka, N. *et al.* Aptamer–field-effect transistors overcome Debye length limitations for small-molecule sensing. *Science* **362**, 319–324 (2018).
43. Lu, C., Jimmy Huang, P.-J., Zheng, J. & Liu, J. 2-Aminopurine Fluorescence Spectroscopy for Probing a Glucose Binding Aptamer. *ChemBioChem* **23**, e202200127 (2022).
44. Danley, R. L. New heat flux DSC measurement technique. *Thermochim. Acta* **395**, 201–208 (2002).
45. Gill, P., Moghadam, T. T. & Ranjbar, B. Differential Scanning Calorimetry Techniques: Applications in Biology and Nanoscience. *J. Biomol. Tech. JBT* **21**, 167–193 (2010).
46. Srivastava, V. K. & Yadav, R. Chapter 9 - Isothermal titration calorimetry. in *Data Processing Handbook for Complex Biological Data Sources* (ed. Misra, G.) 125–137 (Academic Press, 2019). doi:10.1016/B978-0-12-816548-5.00009-5.

47. Jayakumar, K., Bennett, R. & Leech, D. Electrochemical glucose biosensor based on an osmium redox polymer and glucose oxidase grafted to carbon nanotubes: A design-of-experiments optimisation of current density and stability. *Electrochimica Acta* **371**, 137845 (2021).
48. Jain, S. H. Y., Yan He, Parijat. *Handbook of Aqueous Solubility Data*. (CRC Press, 2010). doi:10.1201/EBK1439802458.
49. Price, W. S. Water Signal Suppression in NMR Spectroscopy. in *Annual Reports on NMR Spectroscopy* (ed. Webb, G. A.) vol. 38 289–354 (Academic Press, 1999).
50. Shoara, A. A., Churcher, Z. R., Slavkovic, S. & Johnson, P. E. Weak Binding of Levamisole by the Cocaine-Binding Aptamer Does Not Interfere with an Aptamer-Based Detection Assay. *ACS Omega* **6**, 24209–24217 (2021).
51. Psychogios, N. *et al.* The Human Serum Metabolome. *PLoS ONE* **6**, (2011).
52. Schön, A., Madani, N., Smith, A. B., Lalonde, J. M. & Freire, E. Some Binding-Related Drug Properties are Dependent on Thermodynamic Signature. *Chem. Biol. Drug Des.* **77**, 161–165 (2011).
53. Neves, M. A. D. *et al.* Optimizing Stem Length To Improve Ligand Selectivity in a Structure-Switching Cocaine-Binding Aptamer. *ACS Sens.* **2**, 1539–1545 (2017).
54. Dawood, N. E. Thermodynamic and Kinetic Analysis of Aptamer-Ligand Interactions Using Isothermal Titration Calorimetry. York University, Toronto (2021).
55. Harkness, V., Johnson, P. E. & Mittermaier, A. K. Measuring Biomolecular DSC Profiles with Thermolabile Ligands to Rapidly Characterize Folding and Binding Interactions. *JoVE J. Vis. Exp.* e55959 (2017) doi:10.3791/55959.

## Supplementary Information

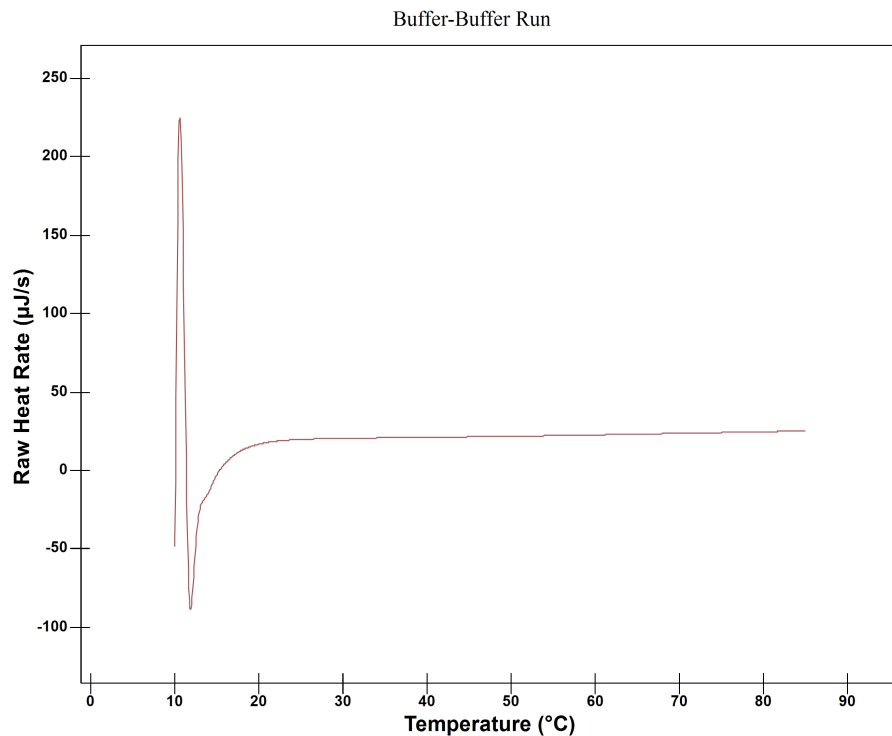


Figure 1: Buffer-Buffer Run. Reference and sample cells loaded with PBS buffer therefore no signal is seen in the thermogram.

### Grubb's Test

Equation is the maximum value in the data set is suspected to be the outlier.

$$G = \frac{x_{max} - \bar{x}}{s}$$

The critical value for the test is

$$G_{critical} = \frac{(n - 1)t_{critical}}{\sqrt{n(n - 2 + t_{crit}^2)}}$$

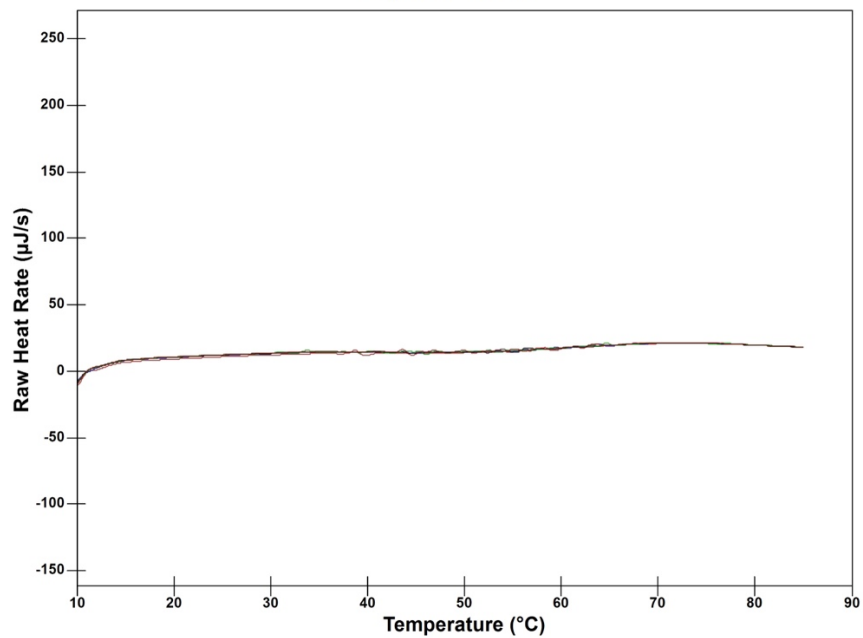


Figure 2: Signal of 110µM OR7 free and bound.